Title:

Cortical granularity shapes the organization of afferent paths to the amygdala and its striatal targets in nonhuman primate

Abbreviated Title: Cortical granularity shapes afferent paths

McHale, AC[1]; Cho, YT[3], *Fudge, JL[1, 2]

University of Rochester, School of Medicine and Dentistry, Departments of Neuroscience[1] and Psychiatry[2], Rochester NY 14642; Yale University, Child Study Center and Department of Psychiatry, New Haven CT 06511[3]

*Correspondence to:

Julie L. Fudge, M.D.

Departments of Neuroscience, and Psychiatry

The Del Monte Institute for Neuroscience

University of Rochester Medical Center

julie_fudge@urmc.rochester.edu

Number of pages: 54

Number of figures: 12

Number of tables: 2

Number of Extended Data Figures: 1

Number of words for abstract: 250 words

Number of words for introduction: 649 words

Number of words for discussion: 1499 words

Conflict of interest statement: The authors declare no competing financial interests.

Acknowledgements: This work was funded through the support of the National Institutes of Mental Health R01MH63291 (J.L.F.), and the Schmitt Program on Integrative Neuroscience (SPIN) GR504304 (J.L.F.). We thank Nanette Alcock for assistance with histology and immunocytochemistry. We also thank Keshov Sharma for R code advice and helpful discussions about data analysis.

Abstract

The prefrontal cortex (PFC) and insula, amygdala, and striatum form interconnected networks that drive motivated behaviors. We previously found a connectional trend in which granularity of the ventromedial and orbital PFC/insula predicted connections to the amygdala, and also the breadth of amygdalo-striatal efferents, including projections beyond the 'classic' ventral striatum. To further interrogate connectional relationships among the cortex, amygdala, and striatum, and to further define the 'limbic (amygdala-recipient) striatum', we conducted tract tracing studies in two cohorts of *Macaques* (Male n = 14, Female n = 1). We focused on the cortico-amygdalo-striatal (indirect) and cortico-'limbic' striatal (direct) paths originating in the entire PFC and insula. Larger data sets and a quantitative approach revealed 'cortical rules' in which cortical granularity predicts the complexity and location of projections to *both* the basal nucleus of the amygdala and striatum. Remarkably, projections from 'cortical-like' basal nucleus to the striatum followed similar patterns. In both 'direct' and 'indirect' paths to the 'limbic' striatum, agranular cortices formed a 'foundational', broad projection, and were joined by inputs from progressively more differentiated cortices. In amygdalo-striatal paths, the ventral basal nucleus was the 'foundational' input, with progressively more dorsal basal nucleus regions gradually adding inputs as the 'limbic striatum' extended caudally. Together, the 'indirect' and 'direct' paths followed consistent principles in which cortical granularity dictated the strength and complexity of projections at their targets. Cluster analyses independently confirmed these connectional trends, and also highlighted connectional features that predicted termination in specific subregions of the basal nucleus and 'limbic' striatum.

Significance Statement

The 'limbic system' broadly refers to brain circuits that coordinate emotional responses. Here, we investigate circuits of the amygdala, which are involved in coding the emotional value of external cues, and their influence on the striatum. Regions of prefrontal cortex and insula form gradients of overlapping inputs to the amygdala's basal nucleus, which feed forward to the striatum. Direct cortical inputs to these 'amygdala-recipient' striatal areas are surprisingly organized according to similar principles, but subtly shift from the classic ventral striatum to the caudal ventral striatum. Together, these distinct subsystems—cortico-amygdala-striatal circuits and direct cortico-striatal circuits—provide substantial opportunity for different levels of internal, sensory, and external experiences to be integrated within the striatum, a major motor-behavioral interface.

Introduction

The prefrontal cortex (PFC) and insula, amygdala, and striatum form interconnected networks that drive motivated behaviors (Van Hoesen et al., 1981; Yeterian et al., 2012). Specific cortical regions project to the amygdala, modulating amygdala neural responses (Klavir et al., 2013; Likhtik et al., 2014). At the same time, these cortical regions and the amygdala form uni-directional inputs to the striatum to mediate goal-directed responses (Haber and Knutson, 2010). This 'triadic' circuitry is implicated in human neuropsychiatric diseases (Akil et al., 2018; Ressler, 2020). Yet, organizational principles of this classic 'limbic' triad are still not completely understood at the cellular level in the nonhuman primate brain.

Although they are separate lobes of cortex, the PFC and insula share a progressive change in cortical laminar differentiation (Mesulam and Mufson, 1982; Barbas and Pandya, 1989). The degree of 'granularity' across the cortical mantle generally refers to the relative presence or absence of 'granular cell' layer IV (Brodmann, 1909; Carmichael and Price, 1994; Petrides and Pandya, 1999, 2002). "Agranular" cortex lacks a granular layer IV, "dysgranular" cortex has an incompletely developed layer IV, and "granular" cortex has a well-differentiated layer IV. Within these broad categories, incremental changes in laminar organization exist, leading to gradual shifts from agranular to dysgranular to granular across the cortical mantle. Classic subdivisions of the PFC and the insula are therefore not independent regions, but rather reflect this continuous laminar organization (Barbas and Garcia-Cabezas, 2016).

The basal nucleus of the amygdala is a key recipient of top-down inputs from the PFC and insula, and is a major output to the striatum (Carmichael and Price, 1995; Ghashghaei and Barbas, 2002; Cho et al., 2013). This nucleus is expanded in primates (Stephan et al., 1987), and has an increased cytoarchitectural complexity along its dorsal-ventral axis. In monkey and human, three large subdivisions of the basal nucleus are recognized: the magnocellular (Bmc), intermediate (Bi,) and parvicellular (Bpc). As their names imply, these dorsally-to-ventrally arranged basal nucleus subdivisions are distinguished by pyramidal cell size and packing density (Braak and Braak, 1983).

Amygdala inputs, particularly from the basal nucleus, are a defining input to the 'classic' ventral striatum, which is involved in forming goal-directed behaviors (Robbins et al., 1989; Popescu et al., 2009). Prior work however has demonstrated basal nucleus projections extend past the 'classic' ventral striatum into caudal aspects of the striatum, which we term the ‘caudal ventral striatum’ (Russchen et al., 1985; Fudge et al., 2002; Cho et al., 2013).

In a previous study examining ‘cortico-amygdalo-striatal’ paths limited to the ventromedial and orbital PFC and insula, we found evidence that relatively higher levels of laminar organization in cortico-amygdala projections governed the topography of cortico-amygdala paths, and was also related to the extent of projections in the next limb of the circuit, the amygdalo-striatal path (Cho et al., 2013). Findings from this study raised subsequent questions around whether the most differentiated dorso-lateral regions of the PFC and insula followed this topography of inputs, and how the topography of cortico-

amygdala-striatal circuits compared to the topography of direct cortico-striatal circuits in striatal regions receiving amygdala input.

Here, we took a systems-based approach to quantitatively compare the organization of 'indirect' cortico-amygdala-striatal circuits and 'direct' cortico-striatal circuits in striatal regions receiving amygdala inputs. We first examined the entire extent of the 'indirect' path, using multiple small injection sites of bi-directional tracer focused on the specific basal nucleus subregions. In the second set of experiments, we placed small injections of retrograde tracer into territories of ‘limbic’ (amygdala-recipient) striatum defined by the first cohort, and compared whether direct cortical-‘limbic’ striatal paths followed similar connectivity principles as indirect paths. Remarkably, we found that a recursive set of hierarchically organized connections, governed by cortical granularity, dictate both the direct and indirect cortical paths to the ‘limbic’ striatum. This organization resulted in unique connectional 'fingerprints' in subregions of the basal nucleus of the amygdala and the 'limbic' (amygdala-recipient) striatum, suggesting functional differences.

Materials and Methods

Study design. Two cohorts of *Macaca fascicularis* (n = 15 total; Male n = 14, Female n = 1, average weight: 4.46 kg, weight range = 3.3 kg - 9.3 kg, average age: 4.51 - 4.64 years, age range = 3 years – 7 years) were used for this study (Labs of Virginia, Three Springs Laboratories, and Worldwide Primates) (Table 1). In the first cohort (Cohort 1, n = 8 animals, all male; see Table 1), a bidirectional tracer injection was placed in various subdivisions of the basal nucleus of the amygdala (Fig. 1). Cohort 1 data includes new

137 analyses in animals used in a previous study (Cho et al., 2013), as well as new cases. To
138 examine the cortico-amygdalo-striatal circuit, we charted and analyzed the number of
139 retrogradely labeled cells in the entire PFC/insula, and the distribution of anterogradely
140 labeled fiber terminals in the striatum. In the second cohort (Cohort 2, n = 8 animals, 1
141 female, 7 males; Table 1), we used anterograde tracing maps from Cohort 1 to guide
142 placement of retrograde tracer injections into the 'limbic' striatum (defined as striatal
143 regions receiving amygdala input). Retrogradely labeled cells in the PFC/insula and in the
144 amygdala were then charted, quantified, and analyzed.
145
146 *Surgical procedures and tissue preparation.* All surgeries were approved by the University
147 of Rochester Committee on Animal Research and follow the National Institutes of Health
148 guidelines. To determine surgical coordinates, some animals had an individualized MRI
149 T2 scan prior to surgery; others had intra-operative electrophysiologic mapping (Fudge
150 et al., 2004; Fudge et al., 2005; Cho et al., 2013; Decampo and Fudge, 2013).
151
152 Monkeys that underwent individualized MRI T2 scans were first administered an
153 intramuscular injection of ketamine (10 mg/kg), then intubated with isofluorane gas during
154 the scanning process. Three days prior to stereotactic surgery, the animals received daily
155 prophylactic pain control with gabapentin (oral dose), which was maintained for 3 days
156 post-operatively. On the day of surgery, monkeys were administered an intramuscular
157 injection of ketamine (10 mg/kg), intubated, and then administered either intravenous
158 pentobarbital (initial dose, 20 mg/kg, i.v.) (for animals undergoing electrophysiologic
159 mapping) or isofluorane gas anesthesia. Once monkeys were placed in a stereotactic

160 head frame, a craniotomy was performed under sterile conditions. For some animals,
161 electrophysiological mapping was conducted first, and electrophysiological features of
162 cells were noted during several penetrations. Injection sites were then plotted for
163 subsequent tracer injections.
164
165 For Cohort 1, the basal nucleus was pressure-injected at various dorsoventral and
166 rostrocaudal sites with either 40 nl of the bidirectional tracers Lucifer yellow conjugated
167 to dextran amine (LY; Invitrogen), Fluorescein conjugated to dextran amine (FS;
168 Invitrogen), or Fluoro-Ruby (tetramethylrhodamine) conjugated to dextran amine (FR;
169 Invitrogen) (Table 1). Antibodies to these tracers do not cross-react, and have similar
170 retrograde and anterograde properties, making them suitable for simultaneous use within
171 the same animal, based on our previous work (Haber et al., 2000; Fudge et al., 2002).
172 For Cohort 2, one striatal site per animal was pressure-injected with 40 nl of wheat germ
173 agglutinin conjugated to horseradish peroxidase (WGA-HRP; Sigma) (Table 1). Following
174 all surgeries, the bone flap was replaced and the overlying tissue sutured. For both
175 cohorts, animals were deeply anesthetized and sacrificed via intracardiac perfusion 10 to
176 12 days after surgery [0.9% saline solution containing 0.5 ml of heparin sulfate followed
177 by cold 4% paraformaldehyde in 0.1M phosphate buffer (PB (0.1M PO_4 pH 7.2)) and 30%
178 sucrose solution for 1 hr)]. After overnight postfixation, brains were cryoprotected in
179 increasing concentrations of sucrose solution (10%, 20%, and 30%). Brains were
180 sectioned coronally on a freezing, sliding microtome at 40 μm, placed in 24 consecutive
181 compartments containing cold cryoprotectant solution (30% sucrose and 30% ethylene
182 glycol in PB), then stored at -20°C (Rosene et al., 1986).

183

184 *Histology*

185 *Immunohistochemistry (ICC).* In both Cohorts, every eighth section through the entire
186 brain was processed using ICC for the relevant tracer. In Cohort 1, adjacent sections
187 through the striatum were processed for calbindin-D28k protein (CaBP) in order to
188 localize the position of anterogradely labeled fibers in striatal subregions (see *Amygdalo-*
189 *striatal path* section in *Cortico-amygdalo-striatal analyses*; **Cohort 1**). In Cohort 2, CaBP-
190 immunoreactivity (IR) in adjacent sections was used to localize tracer injections within
191 striatal subregions (see *Injection site placement;* **Cohort 2**). For all experiments, tissue
192 was rinsed in phosphate buffer with 0.3% Triton-X (PB-TX) overnight. The next day, brain
193 slices were treated with an endogenous peroxidase inhibitor for 5 minutes, and then
194 underwent more rinses in PB-TX. Sections were then pre-incubated for 30 minutes in
195 10% normal goat serum blocking solution with PB-TX (NGS-PB-TX). All sections were
196 then incubated in primary antisera to LY (1:2000; Invitrogen, rabbit), FS (1:2000;
197 Invitrogen, rabbit), FR (1:1000; Invitrogen, rabbit), WGA (1:2500-1:7500 depending on
198 dilution curve; Sigma, rabbit), or CaBP (1:10000; Millipore Bioscience Research
199 Reagents, mouse) at 4°C for four nights. Sections were then thoroughly rinsed, again
200 blocked with 10% NGS-PB-TX, and incubated for 40 minutes in the appropriate
201 biotinylated secondary antibody. After more rinses, sections with bound anti-LY, anti-FR,
202 anti-FS, anti-WGA, or anti-CaBP antibodies were incubated in an avidin-biotin complex
203 (Vectastain ABC kit; Vector Laboratories), and visualized with 3,3'- Diaminobenzidine
204 (DAB), activated with 0.3% hydrogen peroxide (H_2O_2).

205

206 *Cresyl Violet.* In order to localize cortical cytoarchitectonic boundaries for each animal
207 (both Cohorts 1 and 2), we stained 1:24 adjacent or near-adjacent sections for each case
208 with cresyl violet (Chroma-Gesellschaft, West Germany).
209
210 *Acetylcholinesterase (AChE).* In Cohort 1, AChE staining in adjacent sections was used
211 to identify injection site location in the basal nucleus, while in Cohort 2, AChE staining
212 was used to localize tracer-labeled neurons in specific basal nucleus subdivisions. For
213 both, we stained 1:24 adjacent or near-adjacent sections for AChE, using the Geneser-
214 Jensen technique (Geneser-Jensen and Blackstad, 1971).
215
216 *Analysis:*
217 *Cytoarchitectural criteria for the PFC and insula (Fig. 2)*
218 The PFC is defined as the frontal lobe anterior to the arcuate sulcus. Within the PFC, we
219 define the ventromedial and orbital subdivisions according to the nomenclature of
220 Carmichael and Price (Carmichael and Price, 1994), and the dorsomedial (dmPFC),
221 dorsolateral (dlPFC), and ventrolateral (vlPFC) subdivisions according to Petrides et al.
222 (Petrides and Pandya, 1999, 2002). Agranular insula subdivisions were defined
223 according to Carmichael and Price (Carmichael and Price, 1994), and dysgranular and
224 granular insula subdivisions were defined according to Mesulam & Mufson (Mesulam and
225 Mufson, 1982). Regardless of nomenclature, all cytoarchitectural maps of the PFC
226 recognize the gradual transition from agranular to granular laminar organization in the
227 basoventral and mediodorsal direction, based on laminar complexity and the relative
228 development of layer IV (Brodmann, 1909; Preuss and Goldman-Rakic, 1991; Barbas,

229 2007; Nieuwenhuys et al., 2007). The insula similarly progresses from agranular to
230 granular, but in a rostroventral to caudodorsal direction (Mesulam and Mufson, 1982).
231 See Table 2 for descriptions of laminar characteristics of our cytoarchitectural divisions.
232
233 *Categorization of cortical regions by architecture*
234 For quantitative analysis, we categorized cortical areas into either 3 (general) or 9
235 (refined) categories of cortical hierarchy, based on examining layer IV thickness (for 3
236 category granularity) and the extent of layer V sublamination (for 9 category granularity)
237 under Nissl stain (Carmichael and Price, 1994) (Table 2). For 3 category granularity,
238 cortical regions were categorized as agranular cortex if they did not have layer IV,
239 dysgranular if they had incompletely developed layer IV, and granular if they had
240 completely developed layer IV.
241
242 ***Cohort 1.***
243 *Injection site placement.* Relative injection site placement within the Bmc, Bi, and Bpc
244 was determined using adjacent AChE sections for each animal. Throughout the
245 rostrocaudal extent of the basal nucleus, the Bmc is darkly stained with AChE, the Bi has
246 intermediate AChE staining, and the Bpc is lightly stained with AChE, corresponding to
247 the cytoarchitectural gradients in the nucleus (Amaral and Bassett, 1989). All nuclei, and
248 specifically basal nucleus subdivisions, were traced along with landmarks, such as blood
249 vessels across sections, and aligned over tracer-labeled sections in Adobe Illustrator
250 Creative Suite (CS).
251

252 Cases with tracer leakage into overlying structures or white matter tracts were not
253 included in the analysis. To confirm our assessment of injection site placement, we also
254 examined the pattern of retrograde labeling in brain regions known to be a source of
255 afferents to each subdivision. For example, the Bmc receives inputs from the
256 inferotemporal cortex (Herzog and Van Hoesen, 1976), while the Bpc does not; the Bpc
257 receives inputs from the hippocampus in contrast to the Bi and Bmc (Saunders et al.,
258 1988; Fudge et al., 2012).
259
260 *Cortico-amygdalo-striatal analyses*
261 *Cortico-amygdala path.* Retrogradely labeled cells in 1:24 sections were charted through
262 the entire rostral-caudal extent of the PFC and insula using an Olympus AX70 microscope
263 interfaced with Neurolucida via a video CCD (Microbrightfield, Williston, VT). We
264 determined cytoarchitectural boundaries of cortex on adjacent Cresyl violet-stained
265 sections under the microscope, based on criteria described above. These labeled charts
266 were then aligned onto maps of retrogradely labeled cells in Adobe Illustrator CS. The
267 number of retrogradely labeled cells in each cortical subdivision was counted using the
268 Adobe Illustrator "objects" count feature. Cortical subregions were then categorized into
269 3- and 9-category "agranular", "dysgranular", and "granular" groupings as described
270 above (Table 2).
271
272 After assignment of each cortical area to a cortical granularity category, we used the
273 "*circlize"* package in R (R Foundation for Statistical Computing, Vienna, Austria) to
274 generate chord diagrams of our retrograde cortical data, using our 3 and 9 category

classifications of cortical granularity (Gu et al., 2014). Chord diagrams are an effective way to visualize the directionality and connectivity between different nodes of a large data set. ‘Fragments’, which represent each node, are found along the entire perimeter of the chord diagram. The small tic marks and numbers for each ‘fragment’ indicate number of labeled cells. Chord diagrams are organized such that regions containing retrogradely labeled cells (i.e. ‘agranular’ cortex, ‘dysgranular’ cortex, etc.) are located at the top of the diagram as individual ‘fragments’, and injection site locations (i.e. ‘J12LY’, ‘J15LY’, etc.) are located at the bottom of the diagram as individual ‘fragments’. This organization thus reflects the number of retrogradely labeled cells (top axis) associated with specific retrograde injection sites (bottom axis), and the quantitative relationships between the 'strength' of the pathway (number of labeled cells) across cases.

Amygdalo-striatal path. Anterogradely labeled terminal fibers were hand-charted through the rostro-caudal extent of the striatum with the aid of a drawing tube under dark-field illumination. Labeled thick fibers that did not contain boutons were considered fibers of passage and were therefore not included. All hand-drawn charts were then scanned at high resolution and converted in Adobe Illustrator CS for formatting. Striatal boundaries were then determined through comparison to adjacent or near-adjacent CaBP-labeled sections. CaBP-labeled sections were projected onto paper maps of anterogradely labeled fibers in the striatum. Landmarks including blood vessels and fiber tracts were carefully aligned, and CaBP-positive and CaBP-negative areas of the striatum were drawn in. Maps were then scanned into digital format at high resolution, and converted in Adobe Illustrator CS.

298

299 ***Cohort 2.***

300 *Injection site placement.* Injection sites were targeted to the rostral ventral striatum, and
301 also to regions of the ventromedial striatum posterior to the anterior commissure, based
302 on anterograde maps from Cohort 1. Injection site position was determined with
303 reference to adjacent CaBP-labeled sections. In rostral ventral striatal regions, CaBP-
304 poor regions were used to identify the 'shell', while CaBP-rich regions in the rostral ventral
305 striatum were used to identify the 'core' (Meredith et al., 1996; Fudge and Haber, 2002).
306 Collectively, we classify the 'shell' and 'core' as 'classic' ventral striatum. All ventral
307 striatal regions caudal to the level of the 'shell' and 'core' are referred to as 'extended'
308 caudal ventral striatum (Fudge and Haber, 2002). All injection sites that resulted in
309 retrogradely labeled cells in the amygdala were used for cortico-'limbic' striatum and
310 amygdalo-striatal analyses.

311

312 *Amygdalo-striatal path.* The location and quantification of retrogradely labeled cells in
313 basal nucleus subdivisions was mapped in 1:24 sections, with reference to adjacent
314 AChE stained sections. All retrogradely labeled cells in the amygdala were subsequently
315 sorted by subdivision (Bmc, Bi, and Bpc) based on levels of AChE activity and cellular
316 features, and analyzed with respect to position of the injection within the striatum.

317

318 *Cortico-'limbic' striatal path.* Only injection sites resulting in significant numbers of labeled
319 cells in the basal nucleus (>10 cells) were used for these analyses. We quantified
320 retrogradely labeled cells in the entire PFC and insula, and applied the same criteria for

321 classification, analysis, and visualization described for Cohort 1.

322

323 *Comparing cortico-amygdala-striatal and cortico-striatal pathways*. As a way of estimating
324 whether amygdala neuronal populations projecting to different striatal regions received a
325 similar balance of agranular, dysgranular, and granular cortical inputs, we used a 'ratio of
326 ratios' approach to examine data across Cohort 1 (cortico-amygdala) and Cohort 2
327 (amygdala-striatal). While this analysis does not directly examine cortical inputs to
328 amygdala-striatal projections in the same animal, our goal was to examine the proportions
329 of cortical inputs associated with each basal nucleus subdivision. We first pooled the sum
330 of all agranular, dysgranular, and granular labeled cell counts resulting from Bmc, Bi, and
331 Bpc injection sites (i.e. cortico-amygdala data), and converted these sums into
332 percentages. Only basal nucleus injection sites that were wholly confined to one of these
333 subdivisions were used. Once the proportion of labeled neurons in the agranular,
334 dysgranular, and granular cortex were determined for Bmc, Bi, and Bpc injection
335 groupings, we multiplied these percentage values by the number of retrogradely labeled
336 cells in Bmc, Bi, and Bpc resulting from each striatal injection site in Cohort 2. We then
337 converted this sum into a final percentage value to assess the balance of agranular,
338 dysgranular, and granular cortical inputs to amygdalo-striatal projecting cells for each
339 striatal site. We conducted bootstrap analysis to check the 'stability' of our final
340 percentage values in 'indirect' pathway calculations. We did 4 replicates of the data, and
341 found that the average difference of full versus bootstrap data was = 1.4%, the median
342 was 1.0%, the standard deviation was 0.01198, the maximum was 5.6%, and the
343 minimum was 0.1%. This was deemed acceptable. The proportion of labeled cells in the

344 agranular, dysgranular, and granular cortices for the indirect pathway (conjunction of
345 Cohort 1 cortico-amygdala data and Cohort 2 amygdalo-striatal data) were then
346 compared to the proportion of labeled cells in agranular, dysgranular, and granular
347 cortices for each injection site associated with the direct cortico-striatal pathway (Cohort
348 2). Results were expressed as the proportion of labeled neurons in the agranular,
349 dysgranular, and granular cortex associated with each path for each striatal injection site.
350 Sample variance for each granularity grouping and both pathway types was collected and
351 compared.
352
353 *Cluster analysis for cortico-amygdala and cortico-striatal data*: In order to identify cortical
354 subregion connectivity 'fingerprints' of specific basal nucleus and striatal subregions in a
355 quantitative way, we also used k-means cluster analysis on whole cortico-amygdala and
356 whole cortico-striatal retrograde data. K-means cluster analysis is an unsupervised
357 machine learning technique that classifies variables (i.e. retrogradely labeled cells in
358 cortical subregions) into '*k*' groups such that variables with similar characteristics cluster
359 together, while dissimilar variables are clustered in non-overlapping, separate groups
360 (MacQueen, 1967; Kaufman and Rousseeuw, 2009).
361
362 We organized the data matrix rows as we did our chord diagram data, i.e. by ascending
363 granularity grouping (see Table 2) and with cortico-amygdala data matrix columns
364 organized from caudo-ventral to rostro-dorsal injection site location, and cortico-striatal
365 data matrix columns from rostral to caudal injection site location. Cell counts in cortical
366 areas for each injection site were z-scored (using the formula $(x - \mu) / \sigma$ for each injection

site, where x is the number of cells in a specific cortical subregion, μ is the mean cell count of all cortical subregions examined for a specific injection site, and σ is the cell count sample standard deviation of all cortical subregions examined for a specific injection site). Z-scoring (or scaling in general) normalizes the data, which accounts for differences in variance across data points, ensures that cluster plots are not biased by either very high or very low cell count totals, and allows all variables to be considered with equal importance.

In order to approach our clustering in an unbiased manner, and to ensure we were not under- or over-clustering data, we used the 'silhouette method' as a guide to determine the optimal number of '*k*'-clusters to use per data set (Rousseeuw, 1987). The average silhouette width measures how well each variable fits within a cluster; whichever value of *k* is closest to a value of 1 average silhouette width represents high intra-group similarity and high inter-group difference, and was selected as the '*k*' value for that data set. We selected the largest value of *k* that was greater than a 0.5 average silhouette width score.

For all of these analyses, we used the 'tidyverse', 'cluster', and 'factoextra' packages in R Studio. We used the 'set.seed' function to ensure stability and repeatability of our data simulations. We also set 'n.start' to 25, meaning that 25 iterations of our code are run, and the best cluster formatting that results in the lowest within-cluster variation is selected. Datasets and coding information for all data on are deposited on https://figshare.com/s/2ad6809dccb896995407.

390 In order to interpret each cluster, we inspected the patterns of z-scores for each cortical
391 area associated with each cluster. Z-scores were ranked 'high' (mean z-score between
392 1.5001 – 5.5000), 'mean/above mean' (mean z-score between 0.0000 – 1.5000), 'slightly
393 below mean' (mean z-score between -0.0999 - -0.0001), or 'largely below mean' (mean
394 z-score between -0.6000 - -0.1000), based on the distribution of z scores for all cortical
395 regions around the mean. This was done for each pathway. Descriptive names were
396 created for each cluster according to its unique identity.
397

398 **Results**

399 ***Cortico-amygdalo-striatal paths (Cohort 1)***

400 *Basal nucleus injection site placement (Fig. 3)*. In the Bmc, there were three injections
401 placed at slightly different levels—cases J12LY, J16LY, J12FR—as well as five injections
402 at different levels of the Bpc—cases J20LY, J15LY, and J14FR in rostral Bpc, and cases
403 J15FS and J14FS in caudal Bpc, all reported previously (Cho et al., 2013). Three new
404 injections at slightly different levels of the Bi—cases J47FS, J44FR, and J52LY were
405 made and assessed for a more complete survey of the basal nucleus subdivisions. The
406 Bi injection in J47FS was the most ventral, the injection in J52LY extended slightly more
407 dorsally, and the injection in J44FR was most dorsal and lateral, straddling the border
408 with the lateral Bmc.
409

410 *Cortical inputs along basal nucleus subdivisions (Fig. 4)*. After all injections in the basal
411 nucleus, a general pattern emerged in which injection sites placed in the Bpc resulted in
412 many labeled cells in the PFC and insula, restricted to the agranular PFC and insula,

413 while increasingly dorsal and rostral injections in the Bpc, Bi, and Bmc resulted in labeled
414 cells in broader cortical regions, as detailed below.
415
416 *Bpc.* Injection sites in the Bpc (cases J15FS, J14FS, J14FR, J20LY, J15LY) resulted in
417 labeled cells largely confined to agranular PFC, i.e. area 25c, 14c, and agranular insula
418 areas (Fig. 4A). J15FS and J15LY had the most labeled cells in agranular insula
419 subdivisions Iapm and Ial, J14FS had most labeling in Iai and Iapl, J14FR had most
420 labeling in Iapl, and J20LY had most labeling in Ial and Iapl. Across Bpc cases, the
421 majority of labeled cells was in the agranular insula rather than PFC, however, the
422 proportion of labeled cells in the agranular PFC increased gradually as the injection sites
423 were positioned more laterally. Case J15LY, which is an injection in the 'transition'
424 between the Bpc and Bi, had additional labeling in agranular area 24a. J20LY had
425 relatively more labeled cells in dysgranular insula compared to other Bpc sites.
426
427 *Bi.* Bi injections sites (cases J47FS, J52LY, and J44FR) resulted in the majority of labeled
428 cells in agranular cortices, but with a relatively greater contribution of labeled cells in
429 dysgranular and granular cortices compared to Bpc (Fig. 4A). Similar to Bpc, high
430 numbers of labeled cells were found in 25c, 14c, and agranular insula. Case J47FS had
431 the most labeled cells in Iapm and Iai, case J52LY had the majority of labeled cells in Iai
432 and Ial, and case J44FR had the most labeled cells in Iapl. In contrast to Bpc sites, a
433 broader distribution of labeled cells occupied relatively more differentiated agranular
434 areas, including 32c, 24a, 24b, and 13a, as well as labeled cells in dysgranular regions
435 such as area 13b. J44FR, located in a 'transition' region between Bi and Bmc, had

436 relatively more labeled cells in agranular area 24c, dysgranular insula, and 8B, in addition
437 to labeled cells specifically in granular areas 12l and 8Ad.
438
439 *Bmc*. While the majority of labeled cells remained in the agranular regions of PFC and
440 insula, injections in Bmc cases (J12FR, J16LY, and J12LY) had the broadest distribution
441 of labeled cells. Similar to Bpc and Bi, Bmc had many labeled cells in agranular areas
442 25c, 14c, and agranular insula. Similar to Bi cases, Bmc cases had high levels of labeled
443 cells in agranular areas 24a, 24b, and 24c, but in contrast, also had moderate numbers
444 of labeled cells in dysgranular areas 14r, 8B, 13m, and 12o, and some labeled cells in
445 granular areas 45, 9, 8Ad, 8Av, and 46.
446
447 Quantitative analyses revealed that cortical granularity subtype, rather than association
448 with the insula or PFC, predicted inputs across, and even within, basal nucleus
449 subdivisions (Fig. 4B). The agranular cortices in both PFC and insula contained labeled
450 cells after all basal nucleus injections, but were the sole contributor when injection sites
451 were placed in the caudomedial Bpc. Labeled cells in dysgranular cortices appeared and
452 increased in numbers following injections along the rostro-dorsal axis, from the rostro-
453 medial Bpc to Bi to Bmc. Labeled cells in the granular cortices of the insula and PFC
454 formed a relatively smaller contribution, seen only after injections in dorsal Bi and Bmc.
455 The pattern of inputs was nested such that labeled cells in incrementally higher levels of
456 cortical organization only appeared in conjunction with labeled cells in less differentiated
457 cortical areas. Analyses using the more refined (9 category) granularity classification

458 showed a similar, nested pattern (Fig. 4C). In these, subcategories of differentiation
459 within a general granularity 'level' were themselves overlapping in a hierarchical manner.
460
461 ***Basal nucleus-striatal path.*** The distribution and relative density of anterogradely
462 labeled fibers in the striatum from each basal nucleus injection site were mapped (Fig. 5).
463 While all injections sites in the basal nucleus subdivisions resulted in labeled fibers in the
464 shell of the nucleus accumbens, the distribution of labeled fibers varied predictably,
465 expanding its distribution in the striatum as injection site position moved from the
466 caudomedial to rostro-dorsal basal nucleus.
467
468 *Bpc.* Caudomedial Bpc injections (Cases J15FS, J14FS) had labeled fibers largely
469 confined to the dorsomedial shell of the ventral striatum, while more rostral and lateral
470 Bpc injections (J14FR, J20LY, J15LY) resulted in additional labeled fibers in the medial
471 and lateral shell of the ventral striatum, interstitial nucleus of the anterior commissure
472 (IPAC, or fundus striatii), and a small region of the caudomedial putamen caudal to the
473 anterior commissure.
474
475 *Bi.* Bi injection sites (cases J47FS, J52LY, and J44FR) resulted in labeled fibers in the
476 same regions as Bpc inputs, except for the dorsomedial shell (Fig. 5). Compared to Bpc
477 cases, Bi injection sites had additional light distributions of labeled fibers in the central
478 rostral 'core' of the ventral striatum, and moderate to heavy labeled fibers in the ventral
479 body of the caudate nucleus, amygdalostriatal area, ventral putamen posterior to the

480 anterior commissure, and tail of the caudate nucleus. Anterogradely labeled fibers
481 continued caudally to fill the genu of the caudate nucleus.
482
483 *Bmc.* The broad pattern of labeled fibers (cases J12FR, J16LY, and J12LY) resembled
484 those in the Bi, including high densities of labeled fibers in the ventral body of the caudate
485 nucleus, amygdalostriatal area, ventral putamen posterior to the anterior commissure,
486 and tail of the caudate nucleus. Labeled fibers in the rostral ventral striatum were mainly
487 found in the lateral shell, and Bmc injections had more labeled fibers in central domains
488 of the caudate head compared with Bi injections.
489
490 ***Cortico-striatal and amygdalo-striatal paths (Cohort 2)***
491 *Injection site placement*. 8 injections were placed into a range of rostral-caudal striatal
492 regions that received amygdala input based on Cohort 1 anterograde data (Fig. 6). 6
493 sites had large numbers of retrogradely labeled cells in the basal nucleus, and were used
494 for analysis. Of these, 2 injections are located in the rostral ventral striatum; J24WGA
495 was placed in the CABP-negative dorsomedial shell, and J13WGA was placed in the
496 CaBP-positive ventral striatal core. 4 injections are located in more caudal ventral striatal
497 regions; J8WGA, J12WGA, and J11WGA were all placed at different levels of the
498 caudoventral putamen. J41WGA was placed in the ventromedial body of the caudate
499 nucleus posterior to the anterior commissure. 2 injections had relatively few labeled cells,
500 and were classified as control cases (J35FR and J42WGA).
501

502 ***Amygdala inputs delineate 'limbic' striatum regions.*** The basal nucleus had many
503 labeled cells after all injections (Figs. 7A). (Other amygdala nuclei, such as the accessory
504 basal nucleus, had labeled cells in some cases (data not shown), in line with findings from
505 previously published work (Fudge et al., 2002; Cho et al., 2013; Sharma et al., 2020).) In
506 general, the total number of labeled cells in the basal nucleus was highest following rostral
507 ventral striatal injections, decreasing with injections in progressively caudal sites (Fig 7B).
508 With increasingly caudal injection sites, labeled cells also were found in the Bi and Bmc.
509 The pattern of inputs from the basal nucleus subdivisions resembled the hierarchical
510 layering of cortical inputs to the basal nucleus found in Cohort 1. The Bpc formed
511 ubiquitous input to all striatal regions, with additional inputs sequentially added from Bi
512 and Bmc, respectively, in increasingly caudal ventral striatal regions. We termed these
513 caudal regions 'extended' caudal ventral striatum.
514
515 ***Direct cortical inputs to 'limbic' striatum regions.*** All 6 striatal cases contained
516 labeled cells in both the PFC and insula (Fig. 8A). There were labeled cells in the
517 agranular cortex after all injection sites. The injection site in the dorsomedial shell of the
518 striatum resulted in labeled cells almost exclusively in the agranular cortices, while the
519 injection site in the ventral striatal 'core' resulted in additional labeled cells in dysgranular
520 cortices. Injections in more caudal sites of the ventral striatum led to more labeled cells
521 in dysgranular and granular cortices. Overall, the greatest number of labeled cells from
522 the PFC and insula were seen following injections into the rostral ventral striatum, with
523 numbers tapering off following injections in more 'caudal limbic striatum'.
524

525 *‘Classic’ ventral striatum.* Agranular cortices had many labeled cells in cases J24WGA
526 and J13WGA, particularly areas 25c, 25r, 32c, 32r, and agranular insula (Fig. 8A). Both
527 J24WGA and J13WGA had many labeled cells specifically in areas 25 and Iai, but
528 J13WGA, placed in the ventral striatal core, had many additional labeled cells in Ial, as
529 well as many labeled cells in agranular areas 14c and 24b, and dysgranular area 13b.
530
531 *Caudal ventral striatum.* Injections into the caudoventral putamen (J8WGA, J11WGA,
532 and J12WGA) and the ventral body of the caudate head (J41WGA) resulted in labeled
533 cells in the agranular cortices, as did our rostral ventral striatal site (Fig. 8A). The number
534 of labeled cells from agranular cortices decreased along the rostrocaudal axis overall,
535 balanced by increasingly more labeled cells appearing in the dysgranular and granular
536 cortices. For example, cases J8WGA and J12WGA had a majority of cell labeling in
537 agranular insula, but in cases J11WGA and J41WGA agranular insula labeling was more
538 modest, with relatively more labeling in dysgranular insula. Similarly, the number of
539 labeled neurons in agranular area 25 declined along the rostrocaudal axis. All caudal
540 injection sites had many labeled cells in dysgranular insula, and moderate cell labeling in
541 granular insula.
542
543 Quantitative analyses revealed hierarchical, nested projections based on basic levels of
544 cortical differentiation (Fig. 8B). This pattern was similar to that observed in cortico-
545 amygdala retrograde data, with agranular regions containing retrogradely labeled cells
546 for all injection sites, and increasingly caudal regions containing labeled cells in

547 dysgranular and granular cortices of both the insula and PFC. Analyses using a more
548 refined (9 category) granularity classification showed similar patterns (Fig. 8C).
549
550 ***Comparing granularity index for cortico-amygdala-striatal and cortico-striatal***
551 ***pathways***. We used a 'ratio of ratios' approach to estimate how cortical granularity
552 influenced amygdala projections to specific striatal regions in the 'indirect' pathway (see
553 Methods) and compared these results with results for the direct pathway (Fig. 9). For all
554 striatal injection sites, agranular cortical sources dominated in both pathways, followed
555 by a smaller contribution from dysgranular cortices, and the smallest from granular
556 cortices (Fig. 9A). For the indirect pathway, input from each type of cortex remained
557 relatively stable across the rostro-caudal extent of striatal injection sites. In contrast, in
558 the direct pathway there was a shift in the relative contribution from agranular,
559 dysgranular, and granular cortices along the rostrocaudal axis of the amygdala-recipient
560 ('limbic') striatum. In this path, the contribution from agranular cortical regions was
561 progressively reduced, with increasing input from more differentiated cortices. (Fig. 9B &
562 C). Consistent with these trends, there was relatively small variance in the percentage of
563 labeled cells in agranular (29.602), dysgranular (9.975), and granular (5.403) cortex for
564 the 'indirect' path, in contrast to large variances in percentage of labeled cells in the
565 agranular (627.216), dysgranular (300.639), and granular (127.727) cortices depending
566 on the location of the injection site in the striatum (Fig. 9C).
567
568 ***Cortical granularity maps: translating to traditional cortical divisions***

569 After analyzing data using cortical granularity criteria, we were interested in
570 understanding how the combinations of traditional cortical regions comprised these
571 patterns. It has long been known that 'agranular' cortices are associated with the 'limbic'
572 system, while dysgranular cortices are considered 'paralimbic' and the most granular
573 cortices are associated with higher cognitive functions (Badre and D'Esposito, 2009;
574 Barbas, 2015). Since functional studies are typically based on cortical atlas designations,
575 we ‘back-translated’ the granularity index findings by converting the data according into
576 its original atlas designation (Table 2)(Fig. 10).
577
578 In the cortico-amygdala path, the greatest contribution to the 'agranular' cortex was from
579 agranular insula, where the numbers of labeled cells were greater than in all regions of
580 the agranular cortex of the PFC combined (anterior cingulate areas 25, 24, and 32) (Fig
581 10A, blue). The agranular insula was associated with all basal nucleus subdivisions. In
582 the Bpc, agranular insula was surprisingly dominant compared to area 25, especially in
583 more caudomedial regions, based on cell count criteria. Labeled cells in area 25 resulted
584 mainly from injection sites in the rostro-dorsal Bpc as well as the ventral Bi. In a similar
585 manner, the number of labeled cells in areas 24 and 32 increased mainly from Bi and
586 Bmc injection sites, having little association with Bpc injection sites.
587
588 Contributions from dysgranular cortices were mainly from dysgranular area 13,
589 dysgranular area 8 (i.e. area 8B), dysgranular area 12 (i.e. 12o), and the dysgranular
590 insula (Fig. 10A, aqua, green). Area 13 was associated mostly with Bmc injection sites,
591 area 8 associated mostly with dorsal Bi and Bmc injection sites, area 12 associated mostly

592 with dorsal Bi and Bmc injection sites, and dysgranular insula associated with rostral Bpc,
593 dorsal Bi, and Bmc injection sites. In the granular cortices there were modest numbers
594 of labeled cells in regions of the dorsal and lateral PFC (areas 9, 46, 45) and frontal pole
595 (area 10). The granular insula (Ig) had the fewest labeled cells. All of these regions were
596 associated mainly with the dorsal Bi and Bmc.
597
598 In the cortico-striatal path, the agranular cortex as a whole had its largest contribution
599 from the agranular insula, followed by area 25. Labeled cells in the agranular insula were
600 associated with all striatal sites, while labeled cells in area 25 were associated mainly
601 with rostral ventral striatal injection sites. Areas 24 and 32 contained labeled cells in all
602 striatal injection sites, which were prominent in the rostral striatum, but persisted in
603 association with every caudal ventral striatal site. Contributions from the dysgranular
604 component of area 13 (i.e. area 13b) (aqua) and dysgranular insula (light green) were
605 first seen in the core of the rostral ventral striatum, and were present through the caudal
606 ventral striatum. The dysgranular insula (light green) was a key contributor following all
607 caudal ventral striatal injection sites. The number of labeled cells in combined
608 dysgranular/granular (orange/red) cortices was most prominent in area 12 (specifically
609 area 12o), with lesser contributions from other combined dysgranular/granular and fully
610 granular cortices. These findings are consistent with previous work in monkey (Selemon
611 and Goldman-Rakic, 1985; Yeterian and Pandya, 1991; Choi et al., 2017a; Choi et al.,
612 2017b). Labeled cells in all these regions were associated with the core of the rostro-
613 ventral striatum, and caudal ventral striatal sites. The 'core' of the rostral ventral striatum
614 had the most labeled cells overall, compared to other injection sites. Labeled cells from

615 the PFC and insula generally declined in 'extended' caudal ventral striatal regions. These
616 regions receive additional massive inputs from sensory association cortices not examined
617 in this study (Saint-Cyr et al., 1990; Yeterian and Pandya, 1995, 1998) (see Discussion).
618
619 *Cortico-amygdala k-means cluster analysis.* We then took a machine learning approach
620 to examine how granularity-specific cortical subregions project to discrete regions of the
621 basal nucleus and striatum (Fig. 11A-F). For cortico-amygdala retrograde data, we found
622 differences in how cortical regions cluster across the caudal-ventral and rostral-dorsal
623 extent of the basal nucleus, and were able to further examine cluster identities by
624 inspecting tables containing the z-scores of all cortical regions per cluster (Fig. 11A-C,
625 Fig. 11-1.) Four clusters were selected, based on criteria for silhouette analysis. Three
626 different clusters were composed of distinct agranular cortices, and one cluster comprised
627 of multiple agranular, dysgranular, and granular cortices (Fig. 11B & C). The 'Agranular
628 mosaic' cluster (Fig. 11B, green) is an exclusively agranular cluster that contains areas
629 Iapm, 25c, Iai, and Ial. Large z-scores characterized all cortical regions in this cluster
630 (reflecting many retrogradely labeled cells greater than the mean), all of which are
631 associated with all basal nucleus subdivisions. There was a preponderance of 'high' and
632 'mean/above mean' z-scores for retrogradely labeled cells in cortical areas associated
633 with the Bpc and Bi, and some 'mean/above mean' z-scores existing in the Bmc.
634
635 There were two small clusters best defined as 'Basal nucleus topography' clusters (Fig.
636 11B, blue and red). One consisted exclusively of agranular area 24a ('Basal nucleus
637 topography I', teal) and identified the relative dorsal position of the injection in the basal

638 nucleus. The 'Basal nucleus topography I' cluster had labeled cells with increasingly high
639 z-scores ranging from 'largely below mean' z-scores in Bpc sites, to values of ‘high’ z-
640 scores and ‘mean/above mean’ z-scores (i.e. z-scores between 0.0000 - 1.5000) for Bi
641 sites, and ‘high’ z-scores for Bmc sites and the Bi site (J44FR) nearest the Bmc (i.e. z-
642 scores between 1.5001 - 5.5000) (Fig. 11C). In contrast, the 'Basal nucleus topography
643 II' cluster (Fig. 11B, red-orange) was exclusively composed of agranular cortical region
644 Iapl, and was associated with a basal nucleus injection location in the opposite direction,
645 from ventral to dorsal. This small cluster reflected retrogradely labeled cells with ‘high’
646 and ‘mean/above mean’ z-scores for Bpc sites, ‘mean/above mean’ z-scores and ‘slightly
647 below mean’ z-scores (i.e. z-scores between 0.0999 - -0.0001) for Bi sites, and ‘largely
648 below mean’ z-scores for Bmc sites. Together, 'Basal nucleus topography clusters I and
649 II' are inversely related, and gradually increase in their contributions along the ventral-
650 dorsal and dorsal-ventral extent of the basal nucleus, respectively (Fig. 11C).
651
652 The ‘Low-level modulator’ cluster (Fig. 11B, lavender) comprised many agranular,
653 dysgranular, and granular cortical areas which had ‘largely below mean’ z-scores across
654 all basal nucleus injection sites. This cluster describes multiple, low to modest,
655 contributions from labeled neurons in specific cortical projections, the combinations of
656 which define specific basal nucleus subdivisions (Fig. 11C). While all basal nucleus
657 subdivisions received multiple 'low level' inputs, the dysgranular and granular cortices had
658 relatively greater numbers of labeled cells (reflected by z-scores above the mean)
659 associated with the Bi and Bmc compared to the Bpc.
660

661 *Cortico-striatal k-means cluster analysis* (Fig. 11D-F, Fig. 11-1). Using the silhouette
662 method as a guide for selecting an optimal *k*, cortical connectivity with the striatum was
663 best represented through four clusters (Fig. 11D). Similar to cortico-amygdala data,
664 clusters are described after analyzing the z-scores of retrogradely labeled cells in all
665 cortical regions within a cluster, and their relationship to connections with the striatum
666 (Fig. 11E & F). In this dataset, there were two agranular clusters, one
667 agranular/dysgranular cluster, and one cluster containing agranular, dysgranular, and
668 granular inputs (Fig. 11E & F).
669
670 The 'Agranular mosaic' cluster consisted of agranular cortical areas Iai, 32c, 25c, and 25r
671 (Fig. 11E, teal). This cluster revealed key differences between the 'classic' rostral ventral
672 striatum (revealing retrogradely labeled cells in these cortical regions with 'high' and
673 'mean/above mean' z-scores) and the 'extended' caudal ventral striatum, (where the
674 numbers of retrogradely labeled cells were relatively lower, reflected in z-scores 'largely
675 below mean') (Fig. 11F). In the classic ventral striatum shell (J24WGA), area 25c was a
676 strong, defining input, revealed by an exceptionally 'high' z-score for retrogradely labeled
677 neurons, compared to all other regions. Notably, area 25c had weaker input to the core
678 (J13WGA). In sum, the 'Agranular mosaic' cluster differentiated the 'classic' ventral
679 striatum from the 'extended' caudal ventral striatum.
680
681 Inspection of z-scores for a cluster containing the Ial (agranular) and Id (dysgranular),
682 revealed a topographic distribution, leading to its description as a 'Limbic striatal
683 topography' cluster (Fig. 11E, red-orange). Ial projections had 'high' z-scores (i.e. z-

684 scores between 1.5001 - 5.5000) in the classic ventral striatum ‘shell’, which dropped
685 progressively across more caudal ventral striatal sites (Fig 11F). The opposite
686 relationship occurred for Id, where projections associated with caudal ‘extended’ striatal
687 sites (J8WGA, J12WGA, and J11WGA) have ‘high’ z-scores, and progressively drop as
688 injections moved to the ventral caudate (J41WGA) and to classic ventral striatal sites.
689 This inverse rostral-caudal shift from ‘high-low’ Ial influence to ‘low-high’ Id influence
690 occurs posterior to the anterior commissure in the ventral putamen (J8WGA and
691 J12WGA).
692
693 One small cluster consisting of agranular area 24b, was uniquely associated with the
694 injections in the body of the caudate nucleus; we termed it the ‘Ventral caudate identity’
695 cluster (Fig 11E, lavender). This cortical region had an exceptionally ‘high’ z-score in
696 case J41WGA (5.4591), which was substantially lower for all remaining sites (Fig. 11F).
697 This strongly suggests that area 24b is a defining input to the ventral body of the caudate
698 nucleus, relative to other 'limbic striatal' sites.
699
700 Similar to the cortico-amygdala path, there was a ‘Low-level modulator’ cluster for the
701 cortico-striatal path (Fig. 11E, green, 11F). Similar to the cortico-amygdala path, z-scores
702 of retrogradely labeled cells showed relatively modest to weak contribution across
703 agranular, dysgranular and granular cortices for all striatal sites. Also similar to the
704 cortico-amygdala path, while all striatal subdivisions received multiple 'low level' inputs,
705 the dysgranular and granular cortices inputs were shifted, and were associated with
706 relatively greater numbers of labeled cells (reflected by z scores above the mean, purple)

associated with the 'extended' caudal ventral striatum compared to the 'classic' ventral striatum.

Discussion

Several important findings emerged from these studies. The first is that a ‘cortical logic’ governed by laminar structure shapes information flow in both the ‘indirect’ and ‘direct’ paths to the 'limbic' striatum (Fig. 12). Agranular cortical inputs to the basal nucleus of the amygdala and striatum were foundational, as evidenced by the presence of agranular cortical inputs throughout both the cortico-amygdala and cortico-striatal paths. These agranular cortical areas undergird inputs, first from more dysgranular cortex, and then from more granular cortices. In addition, while not a laminar structure, the basal nucleus is cortical-like (Carlsen and Heimer, 1988), and appears to follow hierarchical rules found in cortical projections to the striatum.

Another key result was that cortico-amygdala-striatal paths were generally influenced by a consistent proportion of agranular/dysgranular/granular cortices, overwhelmingly dominated by agranular cortex, regardless of whether the final target was the rostral-ventral or caudal-ventral striatum. In contrast, the ratio of agranular/dysgranular/granular cortical input in the direct cortico-amygdala projection was more variable, and gradually tipped to favor fewer agranular, and more differentiated inputs in the caudal ventral striatum. These results were supported using machine learning approaches in cluster analyses.

730 Finally, we concluded that the ‘limbic’ striatum, as defined by amygdala inputs, extends
731 beyond the 'classic' ventral striatum (nucleus accumbens), as has been previously noted
732 (Russchen et al., 1985; Fudge et al., 2004; Choi et al., 2017a). Different rostrocaudal
733 levels of the ‘limbic’ striatum receive shifting combinations of cortical inputs, making for
734 unique ‘connectional fingerprints’ in each region.
735
736 ***Cortical logic.*** Many individual studies have examined cortico-amygdala, amygdalo-
737 striatal, and cortical-striatal pathways, using anterograde tracer injections (Mufson et al.,
738 1981; Russchen et al., 1985; Goldman-Rakic and Selemon, 1986; Carmichael and Price,
739 1995; Ferry et al., 2000; Ghashghaei and Barbas, 2002; Fudge et al., 2004). Our work
740 builds on these studies by taking a ‘connectomics’-type approach, examining the
741 relationship of multiple pathways within and across animals, and assessing rules by which
742 top-down cortex modulates down-stream targets. This approach is based on a basic
743 tenet that functional specificity is determined by ensembles of afferent projections, and
744 that the strength of any one connection depends on features of the afferents that arrive
745 with it.
746
747 The principles that guide the 'logic’ of cortical afferents are based in the granular
748 complexity of the cortical afferent source. The least differentiated cortical regions
749 examined form a ‘foundational’ base across the basal nucleus and ‘limbic’ (amygdala-
750 recipient) striatum, while inputs from more differentiated cortical regions are additive and
751 are always seen as co-projections with these less differentiated cortical regions. Cluster
752 analyses for both the cortico-amygdala and cortico-striatal paths support this overarching

principle, and also highlighted subtle differences between the pathways. For example, in the cortico-amygdala path, an 'agranular mosaic' cluster revealed strong inputs to all of the basal nucleus. In contrast, in the cortico-striatal path, while agranular cortex projected throughout the striatum, two clusters divided it. The ‘agranular mosaic’ was high only in the 'classic ventral striatum' while the ‘Limbic striatal topography’, consisting of agranular and dysgranular inputs, predicted the location of injection sites along the rostro-caudal axis. In accord with general 'cortical logic', an overlay of multiple dysgranular and granular inputs (‘low-level modulator’ clusters) was a specific feature of each pathway, added only in relatively dorsal (Bmc) or caudal (‘extended’ ventral striatum) sectors.

“Connectivity Fingerprints” and functional anatomic implications

Due to the ‘logic’ of cortical afferents, a predictable, yet unique set of inputs are found in specific subregions of both the basal nucleus and the striatum. Unique connectivity profiles ('fingerprints') are found in ventral-dorsal (basal nucleus) and rostral-caudal (striatum) locations, and shift in a predictable, topographical manner.

Basal nucleus ‘fingerprints’. Against a backdrop of broad-based agranular cortical inputs, projections from increasingly dysgranular and granular cortical regions are added, and overlapped in incrementally dorsal and rostral aspects of the basal nucleus. The 'agranular mosaic’ cluster common to all basal nucleus regions (Iapm, 25c, Iai, Ial) suggests that interoceptive information and autonomic functions modulate the basal nucleus as a whole (Craig, 2002; Wallis et al., 2017). Interestingly, agranular areas 24a and Iapl increase and decrease, respectively, along the Bpc-Bi-Bmc axes, providing a

connectional marker of this gradient (Basal nucleus topography I and II clusters). Areas 24b, 12o, 13b, 8B, 45 (found in the 'low level modulator' cluster) contribute increasingly dysgranular and granular cortical inputs in the Bi and Bmc; these connections are implicated in updating the value of rewards during decision-making (Murray and Rudebeck, 2018).

'Limbic' striatal 'fingerprints' The general connectional rules found are also obeyed in the 'limbic' striatum, but with sharper shifts in cortical inputs, suggesting clear functional changes along the rostrocaudal axis. The classic ventral striatum (also known as the nucleus accumbens) is well-known to mediate reward-driven behaviors (Haber and Knutson, 2010) based in part on amygdala inputs (Popescu et al., 2007; Dallerac et al., 2017). The 'classic' ventral striatum also received massive inputs from 25c, 32c, 25r, Iai (captured in the 'agranular mosaic' cluster), which tapered sharply in the 'extended' ventral striatal sites. Within this agranular cluster, the dorsomedial shell of the nucleus accumbens has a restricted, high input from area 25c, consistent with previous work (Kunishio and Haber, 1994; Chikama et al., 1997). Together, these data inputs from a tight, interconnected cortical network associated with interoceptive processing (Carmichael and Price, 1996) that is important for reward-driven responses.

Agranular cortical inputs found in the classic ventral striatum persist through the caudal ventral ('extended') striatum but decline, as dysgranular and granular cortical inputs are increasingly added. This pattern is captured in the 'Limbic striatal topography' cluster, which shows an increasing input from Id (important for social responses (Jezzini et al.,

799 2012)), review (Evrard, 2019)) with a decreasing input from Iapl, demarcating a gradual
800 connectional boundary between the rostral and caudal ventral striatum. Notably, basal
801 amygdala inputs to the striatum follow similar cortical rules. Bpc projects broadly
802 throughout the 'limbic' striatum, maintaining inputs to the caudal ventral striatum, which
803 are reduced as additional inputs from Bi, and particularly, Bmc enter. Bmc, which itself
804 receives the most differentiated cortical inputs from the orbital and ventrolateral prefrontal
805 cortex (Fig. 12), exclusively projects to the caudal ventral striatum, a recipient of these
806 direct cortical inputs (i.e. areas 24c, 12l, 12o, 45, Id/Ig) (Selemon and Goldman-Rakic,
807 1985; Saint-Cyr et al., 1990; Yeterian and Pandya, 1991; Fudge et al., 2005; Amita et al.,
808 2019). The caudal ventral striatum has long been known as the 'sensory' striatum due to
809 prominent inputs from auditory and visual association cortices in the temporal lobe
810 (Yeterian and Pandya, 1995, 1998). Here we show that these caudal ventral striatal areas
811 also receive inputs from specific cortical areas involved in awareness of bodily
812 movements (Ig, 24c) (Morecraft and Van Hoesen, 1992; Karnath and Baier, 2010; Jezzini
813 et al., 2012) see review (Evrard, 2019) object identification (area 12) (Wilson et al., 1993),
814 and social communication (areas 12l, 45) (Romanski, 2012) via 'indirect' and 'direct'
815 paths. Taken together with established caudal-ventral striatal visual/auditory inputs in
816 primate species, this connectional fingerprint suggests a role in motivated multisensory
817 responses, including complex social interactions.
818
819 Driver/modulators. One way to view the broad ‘foundational’ influence of agranular
820 cortices versus the relatively more restricted influence of differentiated cortices is by
821 applying emerging ideas about differential functions of cortical afferent systems (Sherman

822 and Guillery, 1998). This concept is based on Sherman and Guillery's 'driver-modulator'
823 theory of excitatory afferents, in which a 'driver pathway' provides the main path for
824 information flow and a co-projecting 'modulator pathway' regulates the output from 'driver'
825 systems (Sherman and Guillery, 1998). Applied to our work here, we hypothesize that
826 the agranular cortices comprise driver systems in 'indirect' cortico-amygdala-striatal and
827 'direct' paths due their widespread presence in these target structures. In the 'indirect
828 path', the basal nucleus—itself a 'cortical-like' structure without lamination—projects
829 strongly throughout the 'classic' and 'caudal ventral' striatum, and may be an important
830 'driver'. The other cortical inputs composed of varying combinations of dysgranular and
831 granular cortices point to specific micro-targets along the ventral-dorsal and rostro-caudal
832 axis in both the amygdala and striatum, respectively. These most differentiated cortical
833 regions may be 'modulator' pathways, based on their generally lighter inputs, and the fact
834 that they are always present with denser inputs from less differentiated cortical areas.
835 Specific anatomic and electrophysiologic properties that define 'driver/modulator' paths
836 can be further probed in these systems at the physiologic and anatomic levels (Sherman
837 and Guillery, 1996; Lee and Sherman, 2009; Kelly et al., In Press).
838

839 ***Conclusion***

840 Cortical granularity rules were elucidated in a well-known triad of connections through the
841 'limbic' brain in monkeys. Using a connectomics-type approach, we found that the basal
842 nucleus and 'limbic' striatum are not homogeneous entities, and have unique, predictable,
843 sets of 'connectivity fingerprints' within them. These general connectivity patterns have
844 implications for the ways in which the emotional brain can code increasingly complex

levels of social and cognitive information in a flexible manner, such as predicting actions and choices of others (Saez et al., 2015; Grabenhorst et al., 2019), and may help us to better understand dynamics in complex neuroanatomic circuits associated with human psychiatric disease.

Bibliography

Akil H, Gordon J, Hen R, Javitch J, Mayberg H, McEwen B, Meaney MJ, Nestler EJ (2018) Treatment resistant depression: A multi-scale, systems biology approach. Neurosci Biobehav Rev 84:272-288.

Amaral DG, Bassett JL (1989) Cholinergic innervation of the monkey amygdala: An immunohistochemical analysis with antisera to choline acetyltransferase. J Comp Neurol 281:337-361.

Amita H, Kim HF, Smith MK, Gopal A, Hikosaka O (2019) Neuronal connections of direct and indirect pathways for stable value memory in caudal basal ganglia. Eur J Neurosci 49:712-725.

Badre D, D'Esposito M (2009) Is the rostro-caudal axis of the frontal lobe hierarchical? Nat Rev Neurosci 10:659-669.

Barbas H (2007) Specialized elements of orbitofrontal cortex in primates. Ann NY Acad Sci 1121:10-32.

Barbas H (2015) General cortical and special prefrontal connections: principles from structure to function. Ann Rev Neurosci 38:269-289.

Barbas H, Pandya DN (1989) Architecture and intrinsic connections of the prefrontal cortex in the rhesus monkey. J Comp Neurol 286:353-375.

869 Barbas H, Garcia-Cabezas MA (2016) How the prefrontal executive got its stripes. Curr
870 Opin Neurobiol 40:125-134.
871 Braak H, Braak E (1983) Neuronal types in the basolateral amygdaloid nuclei of man.
872 Brain Res Bull 11:349-365.
873 Brodmann K (1909) “Vergleichende Lokalisationslehre der Grosshirnrinde” (Comparitive
874 Localization Theory of the Cerebral Cortex: Illustrated in its Principles on the Basis
875 of Cell Construction). Leipzig: J.A. Barth.
876 Carlsen J, Heimer L (1988) The basolateral amygdaloid complex as a cortical-like
877 structure. Brain Res 441:377-380.
878 Carmichael ST, Price JL (1994) Architectonic subdivision of the orbital and medial
879 prefrontal cortex in the macaque monkey. J Comp Neurol 346:366-402.
880 Carmichael ST, Price JL (1995) Limbic connections of the orbital and medial prefrontal
881 cortex in macaque monkeys. J Comp Neurol 363:615-641.
882 Carmichael ST, Price JL (1996) Connectional networks within the orbital and medial
883 prefrontal cortex of Macaque monkeys. J Comp Neurol 371:179-207.
884 Chikama M, McFarland N, Amaral DG, Haber SN (1997) Insular cortical projections to
885 functional regions of the striatum correlate with cortical cytoarchitectonic
886 organization in the primate. J Neurosci 17(24):9686-9705.
887 Cho YT, Ernst M, Fudge JL (2013) Cortico-Amygdala-Striatal Circuits Are Organized as
888 Hierarchical Subsystems through the Primate Amygdala. J Neurosci 33:14017-
889 14030.

890 Choi EY, Ding SL, Haber SN (2017a) Combinatorial Inputs to the Ventral Striatum from
891 the Temporal Cortex, Frontal Cortex, and Amygdala: Implications for Segmenting
892 the Striatum. eNeuro 4.
893 Choi EY, Tanimura Y, Vage PR, Yates EH, Haber SN (2017b) Convergence of prefrontal
894 and parietal anatomical projections in a connectional hub in the striatum.
895 NeuroImage 146:821-832.
896 Craig AD (2002) How do you feel? Interoception: the sense of the physiological condition
897 of the body. Nat Rev Neurosci 3:655-666.
898 Dallerac G, Graupner M, Knippenberg J, Martinez RC, Tavares TF, Tallot L, El Massioui
899 N, Verschueren A, Hohn S, Bertolus JB, Reyes A, LeDoux JE, Schafe GE, Diaz-
900 Mataix L, Doyere V (2017) Updating temporal expectancy of an aversive event
901 engages striatal plasticity under amygdala control. Nat Comm 8:13920.
902 Decampo DM, Fudge JL (2013) Amygdala projections to the lateral bed nucleus of the
903 stria terminalis in the macaque: Comparison with ventral striatal afferents. J Comp
904 Neurol 521:3191-3216.
905 Evrard HC (2019) The Organization of the Primate Insular Cortex. Front Neuroanat 13:43.
906 Ferry AT, Ongur D, An X, Price JL (2000) Prefrontal cortical projections to the striatum in
907 macaque monkeys: evidence for an organization related to prefrontal networks. J
908 Comp Neurol 425:447-470.
909 Fudge JL, Haber SN (2002) Defining the caudoventral striatum in primates:
910 cytoarchitectural and histochemical features. J Neurosci 22:10078-10082.
911 Fudge JL, Breitbart MA, McClain C (2004) Amygdaloid inputs define a caudal component
912 of the ventral striatum in primates. J Comp Neurol 476:330-347.

913 Fudge JL, deCampo DM, Becoats KT (2012) Revisiting the hippocampal-amygdala
914 pathway in primates: association with immature-appearing neurons. Neuroscience
915 212:104-119.
916 Fudge JL, Breitbart MA, Danish M, Pannoni V (2005) Insular and gustatory inputs to the
917 caudal ventral striatum in primates. J Comp Neurol 490:101-118.
918 Fudge JL, Kunishio K, Walsh P, Richard C, Haber SN (2002) Amygdaloid projections to
919 ventromedial striatal subterritories in the primate. Neuroscience 110:257-275.
920 Geneser-Jensen FA, Blackstad TW (1971) Distribution of acetyl cholinesterase in the
921 hippocampal region of the guinea pig. Z Zellforsch 114:460-481.
922 Ghashghaei HT, Barbas H (2002) Pathways for emotion: interactions of prefrontal and
923 anterior temporal pathways in the amygdala of the rhesus monkey. Neuroscience
924 115:1261-1279.
925 Goldman-Rakic PS, Selemon LD (1986) Topography of corticostriatal projections in
926 nonhuman primates and implications for functional parcellation of the neostriatum.
927 In: Cerebral Cortex Vol. 5 (Jones EG, Peters A, eds), pp 447-466. New York:
928 Plenum Publishing Corporation.
929 Grabenhorst F, Baez-Mendoza R, Genest W, Deco G, Schultz W (2019) Primate
930 Amygdala Neurons Simulate Decision Processes of Social Partners. Cell 177:986-
931 998 e915.
932 Gu Z, Gu L, Eils R, Schlesner M, Brors B (2014) circlize Implements and enhances
933 circular visualization in R. Bioinformatics 30:2811-2812.
934 Haber SN, Knutson B (2010) The reward circuit: linking primate anatomy and human
935 imaging. Neuropsychopharmacology 35:4-26.

936 Haber SN, Fudge JL, McFarland N (2000) Striatonigrostriatal pathways in primates form
937 an ascending spiral from the shell to the dorsolateral striatum. J Neurosci
938 20(6):2369-2382.
939 Herzog AG, Van Hoesen GW (1976) Temporal neocortical afferent connections to the
940 amygdala in the rhesus monkey. Brain Res 115:57-69.
941 Jezzini A, Caruana F, Stoianov I, Gallese V, Rizzolatti G (2012) Functional organization
942 of the insula and inner perisylvian regions. Proc Natl Acad Sci USA 109:10077-
943 10082.
944 Karnath HO, Baier B (2010) Right insula for our sense of limb ownership and self-
945 awareness of actions. Brain Structure & Function 214:411-417.
946 Kaufman L, Rousseeuw PJ (2009) Finding groups in data: An introduction to cluster
947 analysis, 99 Edition: John Wiley & Sons.
948 Kelly EA, Thomas VK, Indraghanty A, Fudge JL (In Press) Perigenual and subgenual
949 anterior cingulate afferents converge on common pyramidal cells in amygdala
950 subregions of the macaque. J Neurosci.
951 Klavir O, Genud-Gabai R, Paz R (2013) Functional connectivity between amygdala and
952 cingulate cortex for adaptive aversive learning. Neuron 80:1290-1300.
953 Kunishio K, Haber SN (1994) Primate cingulostriatal projection: Limbic striatal versus
954 sensorimotor striatal input. J Comp Neurol 350:337-356.
955 Lee CC, Sherman SM (2009) Modulator property of the intrinsic cortical projection from
956 layer 6 to layer 4. Front Syst Neurosci 3:3.

957 Likhtik E, Stujenske JM, Topiwala MA, Harris AZ, Gordon JA (2014) Prefrontal
958 entrainment of amygdala activity signals safety in learned fear and innate anxiety.
959 Nat Neurosci 17:106-113.
960 MacQueen J (1967) Some methods for classification and analysis of multivariate
961 observations. In: Proceedings of the Fifth Berkeley Symposium on Mathematical
962 Statistics and Probability, pp 281-297. Berkeley, California: University of California
963 Press.
964 Meredith GE, Pattiselanno A, Groenewegen HJ, Haber SN (1996) Shell and core in
965 monkey and human nucleus accumbens identified with antibodies to calbindin-
966 D28k. J Comp Neurol 365:628-639.
967 Mesulam M-M, Mufson EJ (1982) Insula of the Old World Monkey. I: Architectonics in the
968 insulo-orbito-temporal component of the paralimbic brain. J Comp Neurol 212:1-
969 22.
970 Morecraft RJ, Van Hoesen GW (1992) Cingulate input to the primary and supplementary
971 motor cortices in the rhesus monkey: evidence for somatotopy in areas 24c and
972 23c. J Comp Neurol 322:471-489.
973 Mufson EJ, Mesulam MM, Pandya DN (1981) Insular interconnections with the amygdala
974 in the rhesus monkey. Neuroscience 6:1231-1248.
975 Murray EA, Rudebeck PH (2018) Specializations for reward-guided decision-making in
976 the primate ventral prefrontal cortex. Nat Rev Neurosci 19:404-417.
977 Nieuwenhuys R, Voogd J, Huijzen CV (2007) Th Human Central Nervous System: A
978 Synopsis and Atlas, 4 Edition: Springer.

979 Petrides M, Pandya DN (1999) Dorsolateral prefrontal cortex: comparative
980 cytoarchitectonic analysis in the human and the macaque brain and corticocortical
981 connection patterns. Eur J Neurosci 11:1011-1036.
982 Petrides M, Pandya DN (2002) Comparative cytoarchitectonic analysis of the human and
983 the macaque ventrolateral prefrontal cortex and corticocortical connection patterns
984 in the monkey. Eur J Neurosci 16:291-310.
985 Popescu AT, Saghyan AA, Pare D (2007) NMDA-dependent facilitation of corticostriatal
986 plasticity by the amygdala. Proc Natl Acad Sci USA 104:341-346.
987 Popescu AT, Popa D, Pare D (2009) Coherent gamma oscillations couple the amygdala
988 and striatum during learning. Nature Neurosci 12: 801-807.
989 Preuss TM, Goldman-Rakic PS (1991) Myelo-and cytoarchitecture of the granular frontal
990 cortex and surrounding regions in the strepsirhine primate galago and the
991 anthropoid primate macaca. J Comp Neurol 310:429-474.
992 Ressler KJ (2020) Translating Across Circuits and Genetics Toward Progress in Fear-
993 and Anxiety-Related Disorders. Amer J Psych 177:214-222.
994 Robbins TW, Cador M, Taylor JR, Everitt BJ (1989) Limbic-striatal interactions in reward-
995 related processes. Neurosci Biobehav Rev 13:155-162.
996 Romanski LM (2012) Integration of faces and vocalizations in ventral prefrontal cortex:
997 implications for the evolution of audiovisual speech. Proc Natl Acad Sci USA 109
998 Suppl 1:10717-10724.
999 Rosene DL, Roy NJ, Davis BJ (1986) A cryoprotection method that facilitates cutting
1000 frozen sections of whole monkey brains for histological and histochemical

processing without freezing artifact. J Histochem Cytochem Vol. 34, No. 10:1301-1315.

Rousseeuw PJ (1987) Silhouettes: a graphical aid to the interpretation and validation of cluster analysis. J Comput Appl Math 20:53-65.

Russchen FT, Bakst I, Amaral DG, Price JL (1985) The amygdalostriatal projections in the monkey. An anterograde tracing study. Brain Res 329:241-257.

Saez A, Rigotti M, Ostojic S, Fusi S, Salzman CD (2015) Abstract Context Representations in Primate Amygdala and Prefrontal Cortex. Neuron 87:869-881.

Saint-Cyr JA, Ungerleider LG, Desimone R (1990) Organization of visual cortical inputs to the striatum and subsequent outputs to the pallido-nigral complex in the monkey. J Comp Neurol 298:129-156.

Saunders RC, Rosene DL, Van Hoesen GW (1988) Comparison of the efferents of the amygdala and the hippocampal formation in the rhesus monkey: II. Reciprocal and non-reciprocal connections. J Comp Neurol 271:185-207.

Selemon LD, Goldman-Rakic PS (1985) Longitudinal topography and interdigitation of corticostriatal projections in the rhesus monkey. J Neurosci 5:776-794.

Sharma KK, Kelly EA, Pfeifer CW, Fudge JL (2020) Translating fear circuitry: Amygdala projections to subgenual and perigenual anterior cingulate in the Macaque. Cereb Cortex 30:550-562.

Sherman SM, Guillery RW (1996) Functional organization of thalamocortical relays. J Neurophysiol 76:1367-1395.

Sherman SM, Guillery RW (1998) On the actions that one nerve cell can have on another: Distinguishing "drivers" from "modulators". Proc Natl Acad Sci USA 95:7121-7126.

1024 Stephan H, Frahm HD, Baron G (1987) Comparison of brain structure volumes in
1025 insectivora and primates VII. Amygdaloid components. J Hirnforsch 5:571-584.
1026 Van Hoesen GW, Yeterian EH, Lavizzo-Mourney R (1981) Widespread corticostriate
1027 projections from temporal cortex of the rhesus monkey. J Comp Neurol 1981:205-
1028 219.
1029 Wallis CU, Cardinal RN, Alexander L, Roberts AC, Clarke HF (2017) Opposing roles of
1030 primate areas 25 and 32 and their putative rodent homologs in the regulation of
1031 negative emotion. Proc Natl Acad Sci USA 114:E4075-E4084.
1032 Wilson FA, Scalaidhe SP, Goldman-Rakic PS (1993) Dissociation of object and spatial
1033 processing domains in primate prefrontal cortex. Science 260:1955-1958.
1034 Yeterian EH, Pandya DN (1991) Prefrontostriatal connections in relation to cortical
1035 architectonic organization in Rhesus monkeys. J Comp Neurol 312:43-67.
1036 Yeterian EH, Pandya DN (1995) Corticostriatal connections of extrastriate visual areas in
1037 rhesus monkeys. J Comp Neurol 352:436-457.
1038 Yeterian EH, Pandya DN (1998) Corticostriatal connections of the superior temporal
1039 region in rhesus monkeys. J Comp Neurol 399:384-402.
1040 Yeterian EH, Pandya DN, Tomaiuolo F, Petrides M (2012) The cortical connectivity of the
1041 prefrontal cortex in the monkey brain. Cortex 48:58-81.
1042

1043 **Figure legends**

1044 **Table 1:** Injection site summary and monkey characteristics.

1045

1046 **Figure 1:** Study design**.** Cohort 1 animals (bi-directional tracer studies, purple) had a series of

1047 injections placed in different subdivisions of the basal nucleus of the amygdala. Resulting retrogradely
1048 labeled cells in the PFC and Insula were quantified; anterogradely labeled fibers in the striatum were
1049 mapped to guide injections in Cohort 2. Cohort 2 animals (retrograde studies, orange) had a series
1050 of injections placed in different regions of the striatum that were 'amygdala-recipient' (i.e. striatal
1051 regions with labeled fibers in Cohort 1 animals). Retrogradely labeled cells in the amygdala, and the
1052 PFC and Insula, were quantified.

1053

1054 **Figure 2:** Relative levels of cortical lamination in the PFC and Insula in the Macaque. ***A***. Ventral
1055 view ***B***. Sagittal view from the midline ***C***. Lateral view, with lateral fissure 'opened' for ***C'.*** view of
1056 insula. Image adapted from Carmichael & Price, 1994 and Saleem & Price, 2008. The key
1057 illustrates the range of cortical differentiation; shades of blue indicate agranular cortex, shades of
1058 green indicate dysgranular cortex, and shades of red indicate granular cortex. The darker the
1059 shade within each granularity grouping indicates increased development of layer IV, layer II,
1060 and/or layer V of cortex. Insets are from cresyl violet stained sections that give examples of
1061 laminar regions in agranular, dysgranular and granular cortices. Bar = 500 um.
1062 *Abbreviations: 6, area 6 (premotor/supplementary motor area); 8Ad, dorsal area 8A; 8Av,*
1063 *ventral area 8A; 8B, area 8B; 9d, dorsal area 9; 9m, medial area 9; 9/46d, dorsal area 9/46;*
1064 *9/46v, ventral area 9/46; 10m, medial area 10; 10o, orbital area 10; 11l, lateral area 11; 11m,*
1065 *medial area 11; 12l, lateral area 12; 12m, medial area 12; 12o, orbital area 12; 12r, rostral area*
1066 *12; 13a, area 13a; 13b, area 13b; 13l, lateral area 13; 13m, medial area 13; 14c, caudal area*
1067 *14; 14r, rostral area 14; 24a, area 24a; 24b, area 24b; 24c, area 24c; 25c, caudal area 25; 25r,*
1068 *rostral area 25; 32c, caudal area 32; 32r, rostral area 32, 45, area 45; 46, area 46; 9/46d,*
1069 *dorsal area 9/46; area 9/46v, ventral area 9/46; cc, corpus callosum; G, gustatory cortex; Iai,*
1070 *intermediate agranular insula area; Ial, lateral agranular insula area; Iam, medial agranular*
1071 *insula area; Iapl, posterolateral agranular insula area; Iapm, posteromedial agranular insula*

1072 *area; Id, dysgranular insula; Ig, granular insula; ob, olfactory bulb; oc, optic chiasm; PrCO,*
1073 *precentral opercular area.*
1074
1075 **Table 2:** Laminar characteristics of the PFC and insula subdivisions, and 3- and 9-group
1076 granularity assignments. Each column indicates the main granularity grouping of every cortical
1077 area examined (i.e. the relative thickness of layer IV of cortex). The darker the shade within
1078 each sub-section within each column (i.e. 'Agranular 1' vs. 'Agranular 2') represents the
1079 increasing degree of layer V sublamination and/or layer IV development within each granularity
1080 assignment.
1081
1082 **Figure 3:** Schematic of injection site locations in basal nucleus. ***A***. Injection site locations (gray)
1083 in rostro-central Bmc, Bi, and Bpc. ***B***. Injection site locations (gray) in caudal Bpc. ***C***. Dark-field
1084 photomicrograph of injection site location for J16LY, indicated with a white arrow. ***D***. Adjacent
1085 AChE-stained section matched to ***C.*** to localize injection to basal nucleus subdivision (Bmc). ***E***.
1086 Dark-field photomicrograph of the injection site location for J47FS, indicated with a white arrow.
1087 ***F***. Adjacent AChE-stained section matched to ***E.*** to localize injection site within basal nucleus
1088 subdivision (Bi). ***G.*** Dark-field photomicrograph of the injection site location for J15FS, indicated
1089 with a white arrow. ***H.*** Adjacent AChE-stained section matched to ***H.*** to localize injection site
1090 within basal nucleus subdivision (Bpc). Photos taken at 2x magnification. Scale bars = 500 μm.
1091 *Abbreviations: AB, accessory basal nucleus; Bi, intermediate basal nucleus; Bmc, magnocellular*
1092 *basal nucleus; Bpc, parvicellular basal nucleus; L, lateral nucleus; P, putamen; V, ventricle.*
1093
1094 **Figure 4:** Cortico-amygdala path. ***A.*** Representative charts showing the pattern of retrogradely
1095 labeled cells in the PFC and insula resulting from 6 non-overlapping injection sites along the
1096 dorsal-ventral extent of the basal nucleus. ***a'.*** The photomicrograph inset shows an example of

1097 densely concentrated retrogradely labeled cells in the Ial of J15FS. Scale bar = 100 μm ***B.***
1098 Chord diagram showing 3-group quantitative analysis of all retrogradely labeled cells (1:24
1099 sections) through PFC and insula, classified by laminar differentiation. The top axis of this
1100 diagram shows the total number of labeled cells in agranular (blue), dysgranular (green), and
1101 granular (red) cortical areas across all cases examined. The bottom axis shows the number of
1102 labeled cells in agranular, dysgranular, and granular cortices resulting from each basal nucleus
1103 injection site. Injection sites are arranged counter-clockwise from the most caudal-ventral (left)
1104 to most rostral-dorsal injection site location (right). 1 tick mark= 180 cells. ***C.*** Chord diagram
1105 showing 9-group granularity analysis. The top axis shows the total number of labeled cells in
1106 agranular (3 shades of blue), dysgranular (3 shades of green), and granular (3 shades of red)
1107 cortical areas across all cases examined. The darker the shade within each granularity grouping
1108 indicates increased development of layer IV and/or layer V per Table 2. 1 tick mark represents
1109 180 cells.
1110 *Abbreviations: AC, anterior commissure; C, caudate; cc, corpus callosum; GP, globus pallidus;*
1111 *IC, internal capsule; oc, optic chiasm; P, putamen, V, ventricle. For cortical abbreviations, see*
1112 *"Abbreviations" in Figure 2 legend.*
1113
1114 **Figure 5:** Representative charts showing distribution of anterogradely labeled fibers resulting
1115 from the same 6 non-overlapping injection sites shown in Fig. 4, along the dorsal-ventral extent
1116 of the basal nucleus. Injection sites arranged from caudo-medial (Bpc) to rostro-dorsal (Bmc)
1117 across the top. Striatal sections are organized from rostral to caudal levels under each injection
1118 site. Photomicrograph inset shows high density patch of labeled fibers in the caudal ventral
1119 putamen (darkfield). Bar = 500 μm.
1120 *Abbreviations: AC, anterior commissure; C, caudate; C(g), genu of the caudate nucleus; C(t),*
1121 *tail of the caudate nucleus; GP, globus pallidus; GPe; external globus pallidus; GPi, internal*

1122 *globus pallidus; IC, internal capsule; lAstr, lateral amygdalostriatal area; LGN, lateral geniculate*
1123 *nucleus; lIPAC, lateral interstitial nucleus of the posterior limb of the anterior commissure; mAstr,*
1124 *medial amygdalostriatal area; mIPAC, medial interstitial nucleus of the posterior limb of the*
1125 *anterior commissure; OT, optic tract; P, putamen; V, ventricle.*
1126
1127 **Figure 6:** Striatal Injection sites in Cohort 2. ***A. - D.*** Schematics of retrograde injection site
1128 locations from rostral (A) to progressively caudal regions (B-D). Medium gray sites (solid lines)
1129 depict injections with significant labeled cells in amygdala, included for analysis; light gray sites
1130 (dotted lines) resulted in few labeled cells in the amygdala. ***E-F.*** Brightfield photomicrographs in
1131 the classic ventral striatum. ***E***. Injection site location in dorsomedial shell, with adjacent CaBP-
1132 stained section (***E'.***) showing injection alignment in CaBP-negative shell**.** ***F.*** Injection site in the
1133 rostral 'core', with adjacent CaBP-stained section (**F'**.) showing shell/core boundary. ***G-J.***
1134 Caudal 'limbic' striatum injection sites. ***G.*** caudoventral putamen at the level of the anterior
1135 commissure, ***H.*** caudoventral putamen posterior to the anterior commissure. ***I.*** ventral body
1136 of caudate nucleus**.** ***J.*** Injection site location in caudomedial putamen at the level of the
1137 hippocampus. Scale bars = 1mm.
1138 *Abbreviations: AC, anterior commissure; C, caudate; Co, ventral striatum core; GPe; external*
1139 *globus pallidus; GPi, internal globus pallidus; IC, internal capsule; P, putamen; Sh, ventral*
1140 *striatum shell.*
1141
1142 **Figure 7:** Amygdalo-striatal path. ***A.*** Charts of retrogradely labeled cells through the
1143 rostrocaudal basal nucleus following striatal injections in Cohort 2. Injection sites arranged from
1144 rostral (top) to caudal (bottom). All 6 cases resulted in many retrogradely labeled cells in the
1145 basal nucleus. Cell labeling in other nuclei (shaded in gray) is not shown for clarity. ***B.*** Chord
1146 diagram showing numbers of labeled cells in the Bpc, Bi, and Bpc by injection site placement.
1147 The top axis of this diagram shows the total number of labeled cells in Bpc (cyan), Bi (fuchsia),

1148 and Bmc (purple) across all cases examined. The bottom axis shows the number of labeled cells
1149 in each basal nucleus subdivision resulting from each striatal injection site, and is arranged
1150 counter-clockwise from the most rostral (left) to most caudal (right) injection site location. Each
1151 tick mark for both the top and bottom axes = 60 cells.
1152
1153 **Figure 8:** Cortico-'limbic' striatal path. ***A.*** Representative charts depicting retrogradely labeled
1154 cells in the PFC and insula after injections in various striatal regions along the rostral-caudal
1155 extent of the 'limbic' striatum. Cases J24WGA and J13WGA had injections in shell and core of
1156 the 'classic' ventral striatum, respectively. Injection sites in J8WGA, J12WGA, J41WGA, and
1157 J11WGA were placed in different parts of the 'extended' ventral striatum. ***B.*** Chord diagram
1158 showing the number of retrogradely labeled cells (1:24 sections) in agranular (blue), dysgranular
1159 (green), and granular (red) cortical areas across all cases examined (top axis). The bottom axis
1160 shows the number of labeled cells found in agranular, dysgranular, and granular cortices after
1161 each striatal injection site. The bottom axis is arranged counter-clockwise from the most rostral
1162 (left) to the most caudal (right) injection site location. Each tick mark represents 400 cells. ***C***.
1163 Chord diagram using 9-group granularity analysis. following the same color schema in **Figure**
1164 **4C.** Each tic mark for both the top and bottom axes represents 400 cells.
1165
1166 **Figure 9:** Indirect and direct pathway analysis**.** ***A.*** Composite diverging bar plots of each striatal
1167 injection showing the proportion of labeled cells in agranular (blue), dysgranular (green) and
1168 granular (red) cortices after calculating indirect pathway and direct pathway labeled cells. The
1169 proportion of labeled cells associated with amygdala inputs to all striatal sites ('indirect' path) is
1170 relatively consistent with a large percentage of cells categorized as agranular, and consistently
1171 small percentages of labeled cells categorized as dysgranular and granular, respectively. In
1172 contrast, the 'direct' cortico-'limbic' striatal path shows more variation with rostral ventral striatal
1173 sites having the greatest proportion of labeled cells in agranular cortices, and relatively small

contributions from the dysgranular and granular cortices. This balance shifts at progressively caudal ventral levels, with reductions in labeled cells in agranular cortices, and incrementally more labeled cells in dysgranular cortices > granular cortices. ***B.*** Individual cases plotted for each path. ***C.*** Boxplots of agranular (blue), dysgranular (green) and granular (red) percentage data for indirect (dark shades) and direct (light shades) pathway data, illustrating differences in variance between granularity classes in the 'indirect' and 'direct' paths.

Figure 10: ***A.*** Quantitative analysis of retrograde cortico-amygdala cell labeling in cortical areas (see text). The top axis shows the total number of labeled cells in each cortical area examined. Blue = agranular cortex only; blue-green = mix of agranular and dysgranular cortices, green = dysgranular cortex only; orange = mix of dysgranular and granular cortices, and red = granular cortex only. The top axis of this diagram shows the number of labeled cells from each cortical area resulting from each basal nucleus injection site. The bottom axis shows the number of labeled cells in each cortical region, per injection site. Each tic mark for both the top and bottom axes represents 180 cells. ***B.*** Quantitative analysis of retrograde cortico-striatal cell labeling by cortical area, indicated on the top axis, with the same color schema in ***A.***. The bottom axis shows the number of labeled cells in each cortical region, resulting from each striatal injection site. Each tic mark for both the top and bottom axes represents 400 cells.

Figure 11: K-means cluster analyses for cortico-amygdala (A-C) and cortico-striatal (D-F) data. ***A***. Silhouette plot for cortico-amygdala data. ***B.*** K-means cluster analysis plot for cortico-amygdala data. Each axis represents the percentage of the data captured in the two dimensions that account for the highest variance across the data. 4 clusters are named by descriptive labels, based on which feature of the data they capture: ‘Basal nucleus topography I’ (teal), ‘Agranular mosaic’ (green), ‘Basal nucleus topography II’ (red-orange), and ‘Low-level modulator’ (lavender). ***C.*** Cortico-amygdala cluster identities, based on inspection of z-scores across each

1200 cluster. Table columns are organized from caudal-ventral to rostral-dorsal injection site location.
1201 Z-scores are grouped from 'high' to 'low' values: 'high' = mean z-score between 1.5001 – 5.5000
1202 (dark purple), 'mean/above mean' = mean z-score between 0.0000 – 1.5000 (light purple),
1203 'slightly below mean' = mean z-score between -0.0999 - -0.0001 (light orange), and 'largely
1204 below mean' = mean z-score between -0.6000 - -0.1000 (dark orange). ***D.*** Silhouette plot for
1205 cortico-striatal data. ***E.*** K-means cluster analysis plot for cortico-striatal data, with 4 clusters
1206 identified by descriptive labels: 'Limbic striatal topography' (red-orange), 'Agranular mosaic'
1207 (teal), 'Ventral caudate identity' (lavender), and 'Low-level modulator' (green). ***F.*** Cortico-striatal
1208 cluster identities, based on inspection of the distribution of z-scores for each cluster. Extended
1209 data Figure 11-1 shows a table listing the mean and standard deviation for cell counts for each
1210 injection site for calculating z-scores.
1211
1212 **Figure 11-1:** Means and standard deviations of total labeled cortical cell counts found for each
1213 basal nucleus and striatal injection site.
1214
1215 **Figure 12:** Overview of 'cortical logic' in the 'indirect' pathway (PFC/Insula → amygdala
1216 connectivity, left + amygdala → 'limbic' striatum connectivity , bottom) and the 'direct' pathway
1217 (PFC/Insula → 'limbic' striatum connectivity, right).

Table 1: Injection site summary and monkey characteristics					
Monkey Identification	Number of injections	Injection type	Cohort Affiliation	Weight (kg)	Age (years)
J14	2	FR FS	Cohort 1 Cohort 1	3.3	4
J15	2	LY FS	Cohort 1 Cohort 1	3.3	3-4*
J16	1	LY	Cohort 1	3.6	3-4*
J20	1	LY	Cohort 1	9.3	7
J44	1	FR	Cohort 1	4.4	4.2
J47	1	FS	Cohort 1	4.6	5.3
J52	1	LY	Cohort 1	4.1	3.5
J12	3	LY FR WGA	Cohort 1 Cohort 1 Cohort 2	6	6.6
J8+	1	WGA	Cohort 2	3.5	4.2
J11	1	WGA	Cohort 2	4.1	4.5
J13	1	WGA	Cohort 2	3.8	3.9
J24	1	WGA	Cohort 2	3.9	4.9
J35**	1	FR	Cohort 2	4.5	3.6
J41	1	WGA	Cohort 2	4.1	5.8
J42**	1	WGA	Cohort 2	4.4	4.1

"+" female monkey

"*" approximate age

"**"control injections

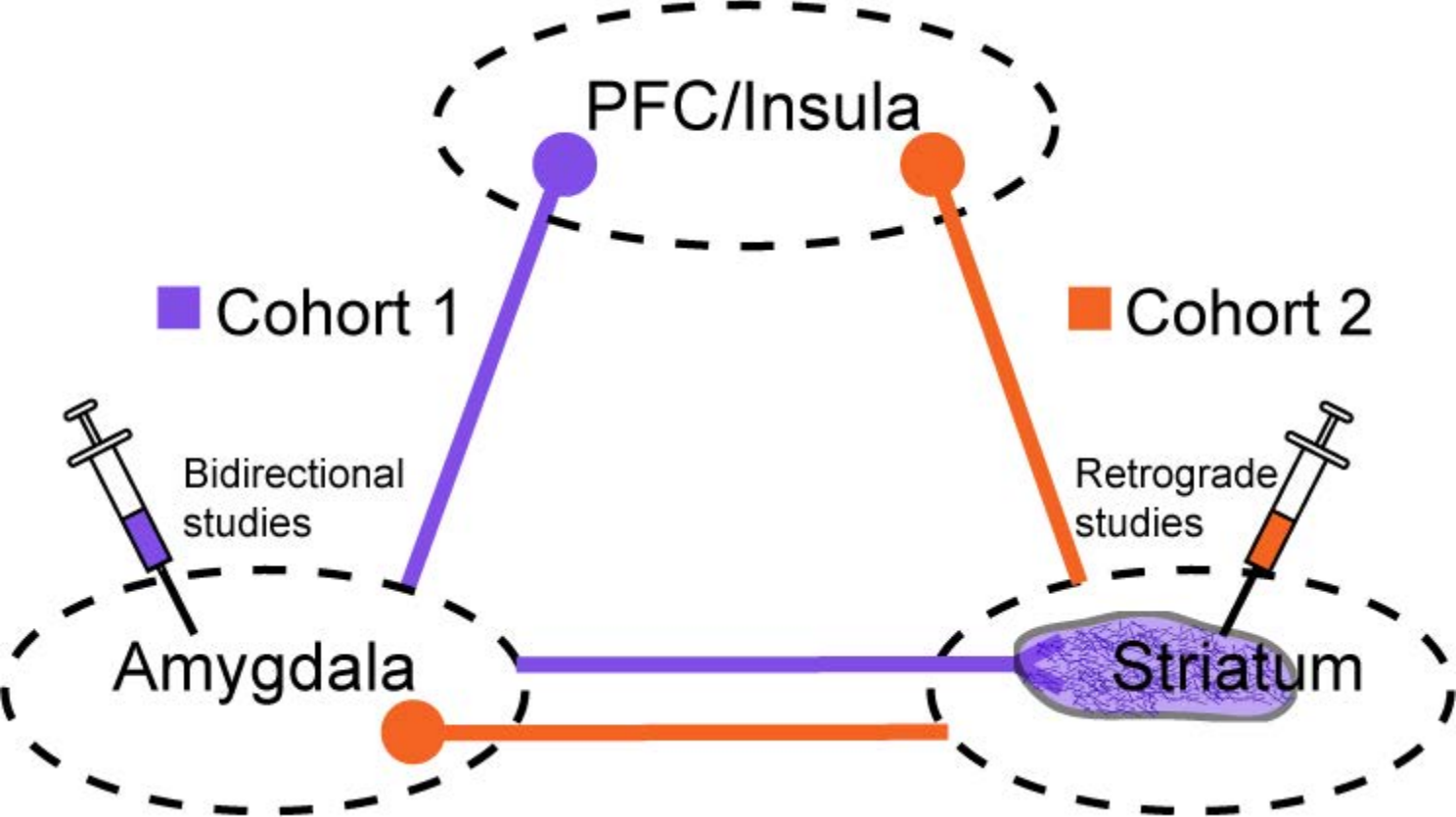
PFC/Insula
Cohort 1
Cohort 2
Bidirectional studies
Retrograde studies
Amygdala
Striatum

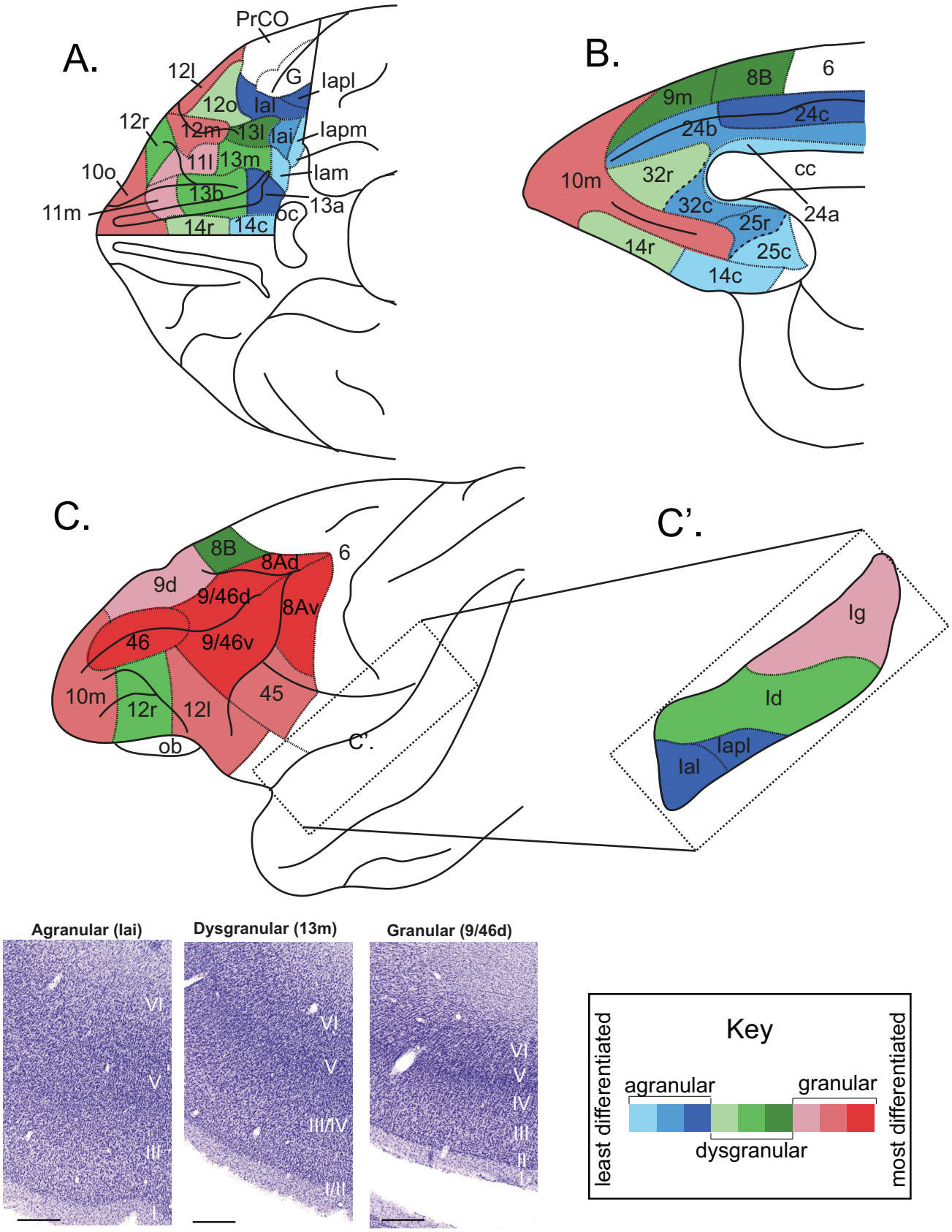
A.
PrCO
12l
G
lapl
12o
lal
12r
12m
13l
lai
lapm
11l
13m
10o
lam
13b
11m
13a
oc
14r
14c
B.
8B
6
9m
24c
24b
10m
32r
cc
32c
24a
25r
14r
25c
14c
C.
8B
8Ad
6
9d
9/46d
8Av
46
9/46v
10m
12r
12l
45
ob
C'.
C'.
Ig
Id
lapl
lal
Agranular (lai)
Dysgranular (13m)
Granular (9/46d)
VI
V
III
I
VI
V
III/IV
I/II
VI
V
IV
III
II
I
Key
agranular
granular
dysgranular
least differentiated
most differentiated

Table 2: Rationale for 3- and 9-group granularity assignments

Agranular	
Granularity Grouping	Reason for granularity grouping
Agranular 1	
Iam	No layer IV, and no layer V sublamination. (Carmichael & Price, 1994)
Iapm	No layer IV, and no layer V sublamination. (Carmichael & Price, 1994)
25c	No layer IV, less developed compared to 32c, 32r, and 25r. (Carmichael & Price, 1994)
24a	Has only 4 cortical layers and rudimentary lamination. (Carmichael & Price, 1994)
14c	Has only 4 cortical layers. (Carmichael & Price, 1994)
Agranular 2	
32c	No layer IV; Caudal 32 resembles 25r; has horizontal striations of pyramidal cells in layer V. (Carmichael & Price, 1994)
25r	No layer IV; caudal 32 resembles 25r. (Carmichael & Price, 1994)
24b	No layer IV; has more prominent vertical striations in layer V compared to 24c. (Carmichael & Price, 1994)
Iai	No layer IV; has partially sublaminated layer V; superficial layer V has row of large pyramidal cells. (Carmichael & Price, 1994)
Agranular 3	
Ial	No layer IV; layer V is sublaminated. (Carmichael & Price, 1994)
Iapl	No layer IV; layer V is sublaminated. (Carmichael & Price, 1994)
13a	No layer IV; layer V is sublaminated. (Carmichael & Price, 1994)
24c	No layer IV; Has pyramidal cell aggregates in layer V. (Carmichael & Price, 1994)

Dysgranular	
Granularity Grouping	Reason for granularity grouping
Dysgranular 1	
32r	Is more developed than 32c and 25r and is slightly dysgranular (Carmichael & Price, 1994). No layer V sublamination.
12o	Very weakly staining layer IV, no layer V sublamination. (Carmichael & Price, 1994)
14r	Has distinct small cells in layer II, no horizontal or vertical striations in layer V. (Carmichael & Price, 1994)
Dysgranular 2	
13b	Has horizontal and vertical striations in layer V. (Carmichael & Price, 1994)
12r	Has vertical striations in layer V, but it is not sublaminated. (Carmichael & Price, 1994)
13m	Has a sparse granular layer. Has no/less distinct sublamination of layer V (and layer III). (Carmichael & Price, 1994)
Id	Has thin layer IV with clusters of granular cells interrupted by pyramidal cells. No layer II. Almost identical in appearance to dysgranular component of caudal OFC. (Mesulam & Mufson, 1982)
Dysgranular 3	
13l	Has poorly developed layer IV and has clearly sublaminated layer V. (Carmichael & Price, 1994)
8B	Layer II is well defined; Layer IV is poorly developed and layer V blends with layer VI, but layer V is sublaminated (it has a few darkly stained cells in layer Va). (Petrides & Pandya, 1999)
9m	Has a more narrow and cell sparse layer IV than 9. (Petrides & Pandya, 1999)

Granular	
Granularity Grouping	Reason for granularity grouping
Granular 1	
9d	Has a narrow layer IV. Layer Va has deeply pigmented cells and layer Vb blends with layer VI. (Petrides & Pandya, 1999)
Ig	Layer II has moderately advanced granularity, and layer IV has prominent granularity. Layer V and VI are not fully differentiated from each other; (Layer III is bilaminate). (Mesulam & Mufson, 1982)
11m	Granular with bilaminate layer V. Layer V is thinner and more trilaminate than in 13m. Outer and inner sublaminae are broken into aggregates of neurons. (Carmichael & Price, 1994)
11l	Granular with bilaminate layer V containing aggregates of pyramidal cells. Layer V is thinner and more trilaminate than in 13m. Does not have outer and inner sublaminae broken up into neuron aggregates. (Carmichael & Price, 1994)
Granular 2	
10o	Is more granular than 11m and 11l, but layer IV not as clear. Layer V is thinner than in 11m or 11l; contains vertical and horizontal striations in layer V, and layer V is thinner than 11l and 11m. (Carmichael & Price, 1994)
10m	Has completely developed II and IV; has horizontal and vertical striations in layer V. Layer IV is more granular than 11m and 11l but not well demarcated, thin layer V with radial striations. (Carmichael & Price, 1994)
12m	Has completely developed II and IV; has clearly sublaminated layer V. Is more granular than 12r, 13l, and 12o. (Carmichael & Price, 1994)
12l	Has completely developed layers II and IV; has prominent/sharp sublamination of layer V. (Carmichael & Price, 1994)
45	Well developed layer IV with medium sized layer V (also has distinct and uniquely thick layer III). (Petrides & Pandya, 2001)
Granular 3	
8Av	Layer IV is broad and densely packed with small neurons (Layer II is also developed and densely packed). Layer V is less dense, but is bilaminate. Resembles 8Ad, but layer IV is broader, and layer III pyramidal neurons are more densely packed. (Petrides & Pandya, 1999)
8Ad	Layer IV is broad and densely packed with small neurons (Layer II is also developed and densely packed). Layer V is less dense, but is bilaminate. Resembles 8Av, but layer IV is less broad, and layer III pyramidal neurons are less densely packed. (Petrides & Pandya, 1999)
46	Layer IV is well developed; layer V is sublaminated (layer Va has small number of deeply stained cells and layer Vb blends with layer VI). (Petrides & Pandya, 1999)
9/46d	Similar features as 46, but layer III has large and darkly stained pyramidal neurons; Located dorsally. (Petrides & Pandya, 1999)
9/46v	Similar features as 46, but layer III has large and darkly stained pyramidal neurons; Located ventrally. (Petrides & Pandya, 1999)

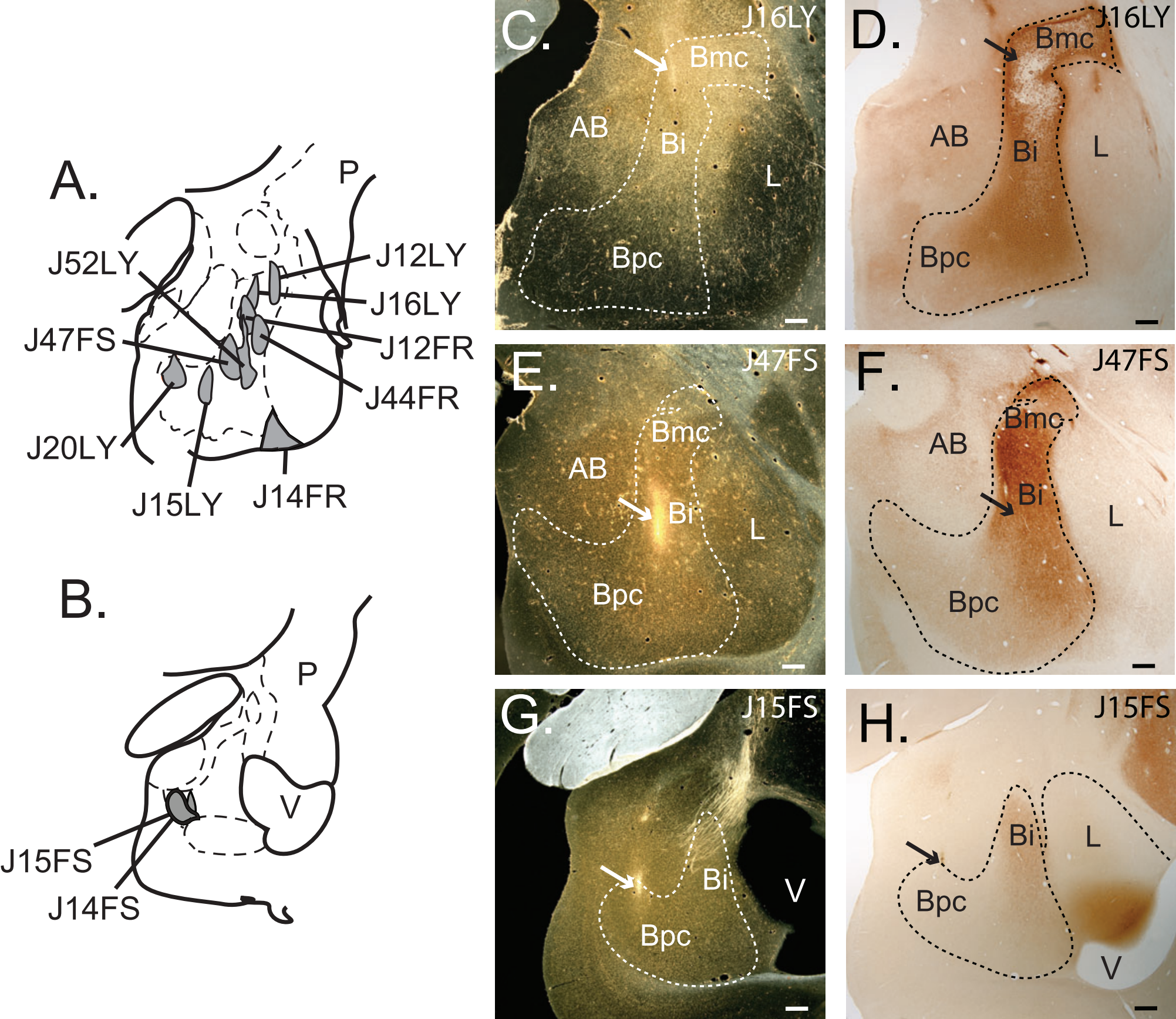
A.
P
J52LY
J12LY
J16LY
J47FS
J12FR
J44FR
J20LY
J15LY
J14FR
B.
P
V
J15FS
J14FS
C.
J16LY
Bmc
AB
Bi
L
Bpc
D.
J16LY
Bmc
AB
Bi
L
Bpc
E.
J47FS
Bmc
AB
Bi
L
Bpc
F.
J47FS
Bmc
AB
Bi
L
Bpc
G.
J15FS
Bi
V
Bpc
H.
J15FS
Bi
L
Bpc
V

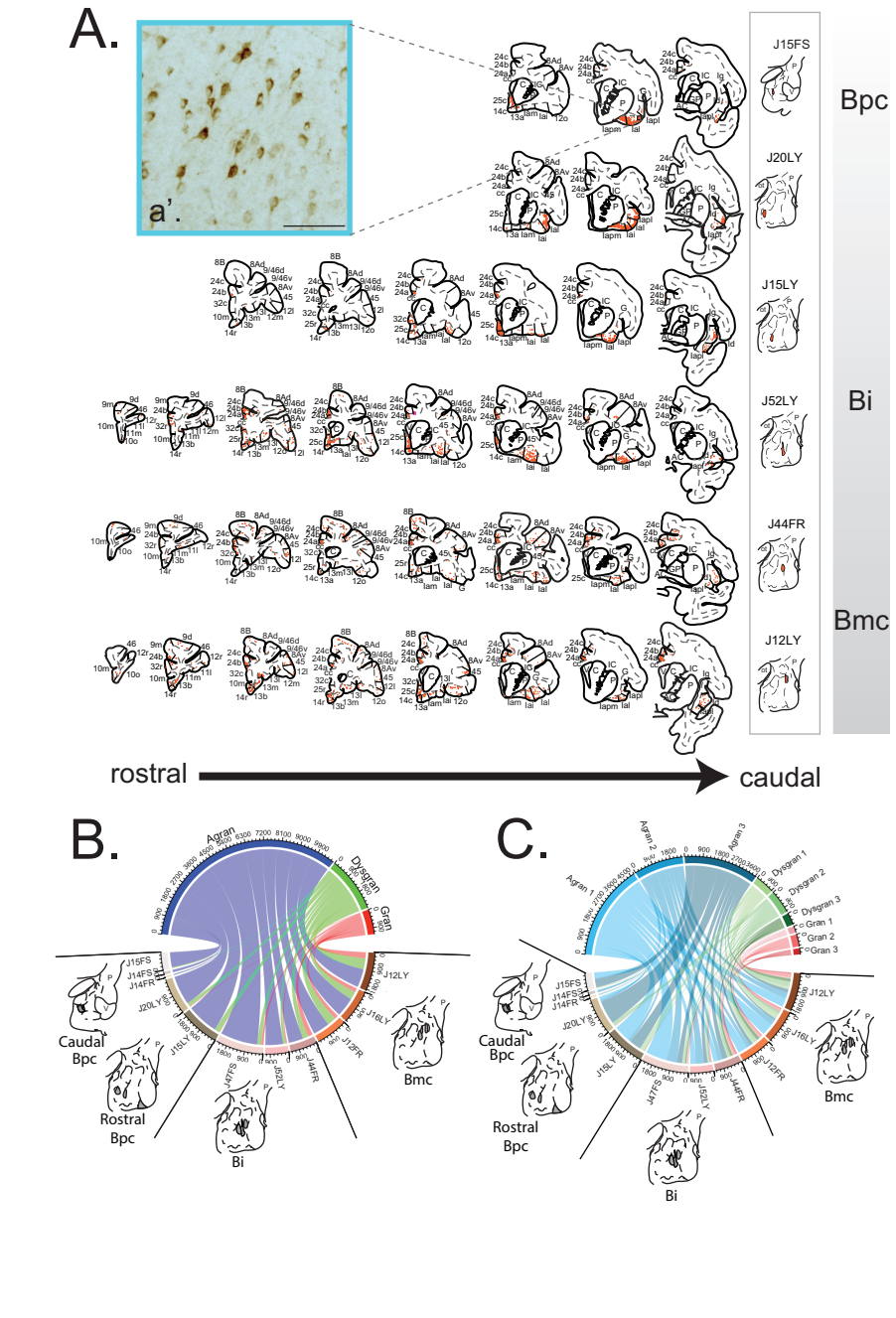
A.
a'.
J15FS
J20LY
J15LY
J52LY
J44FR
J12LY
Bpc
Bi
Bmc
rostral
caudal
B.
Agran
Dysgran
Gran
Caudal Bpc
Rostral Bpc
Bi
Bmc
C.
Agran 1
Agran 2
Agran 3
Dysgran 1
Dysgran 2
Dysgran 3
Gran 1
Gran 2
Gran 3
Caudal Bpc
Rostral Bpc
Bi
Bmc

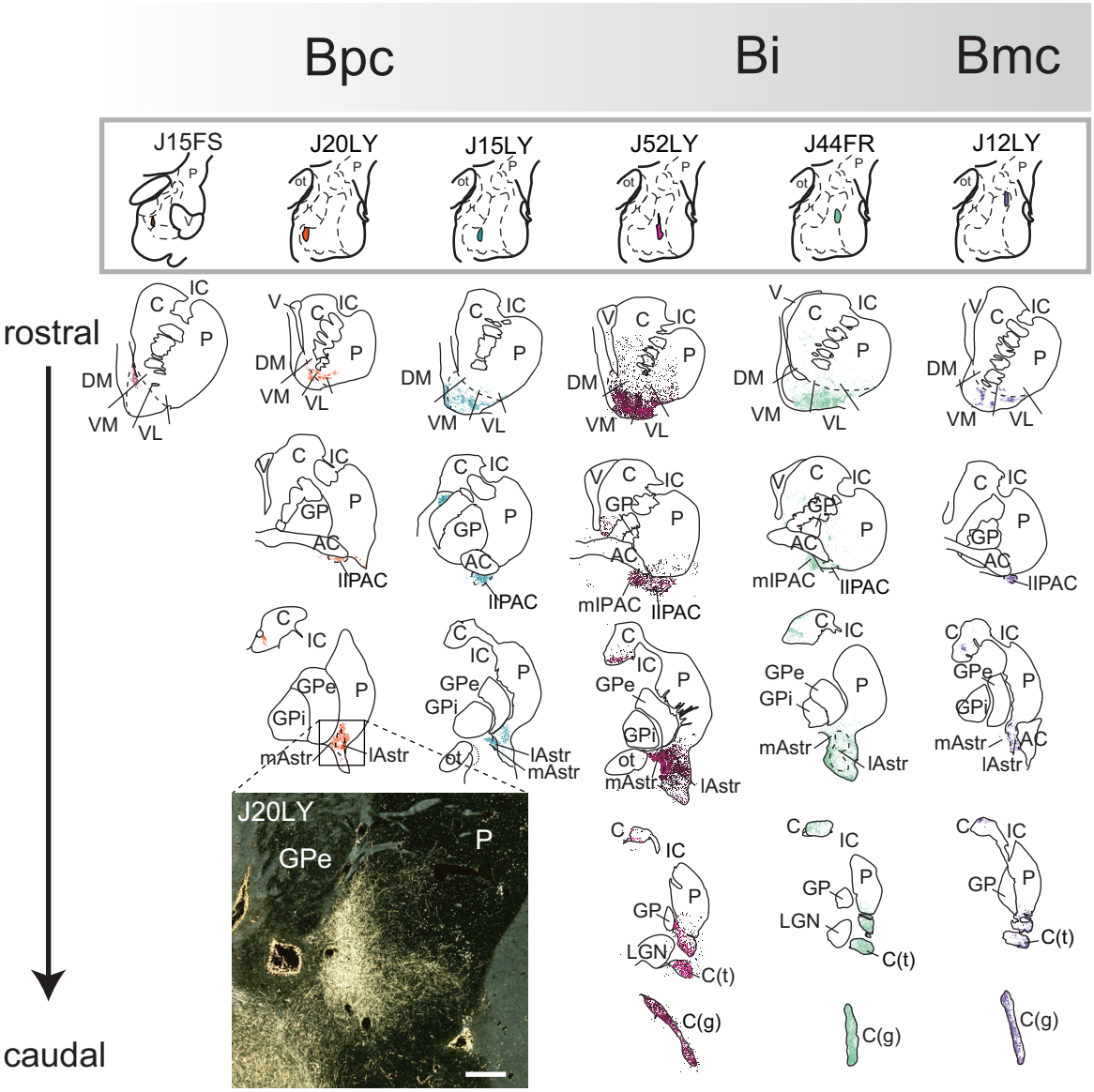
Bpc
Bi
Bmc
J15FS
J20LY
J15LY
J52LY
J44FR
J12LY
rostral
caudal
IC
C
P
DM
VM
VL
V
GP
AC
lIPAC
mIPAC
GPe
GPi
mAstr
lAstr
ot
LGN
C(t)
C(g)
J20LY
GPe
P

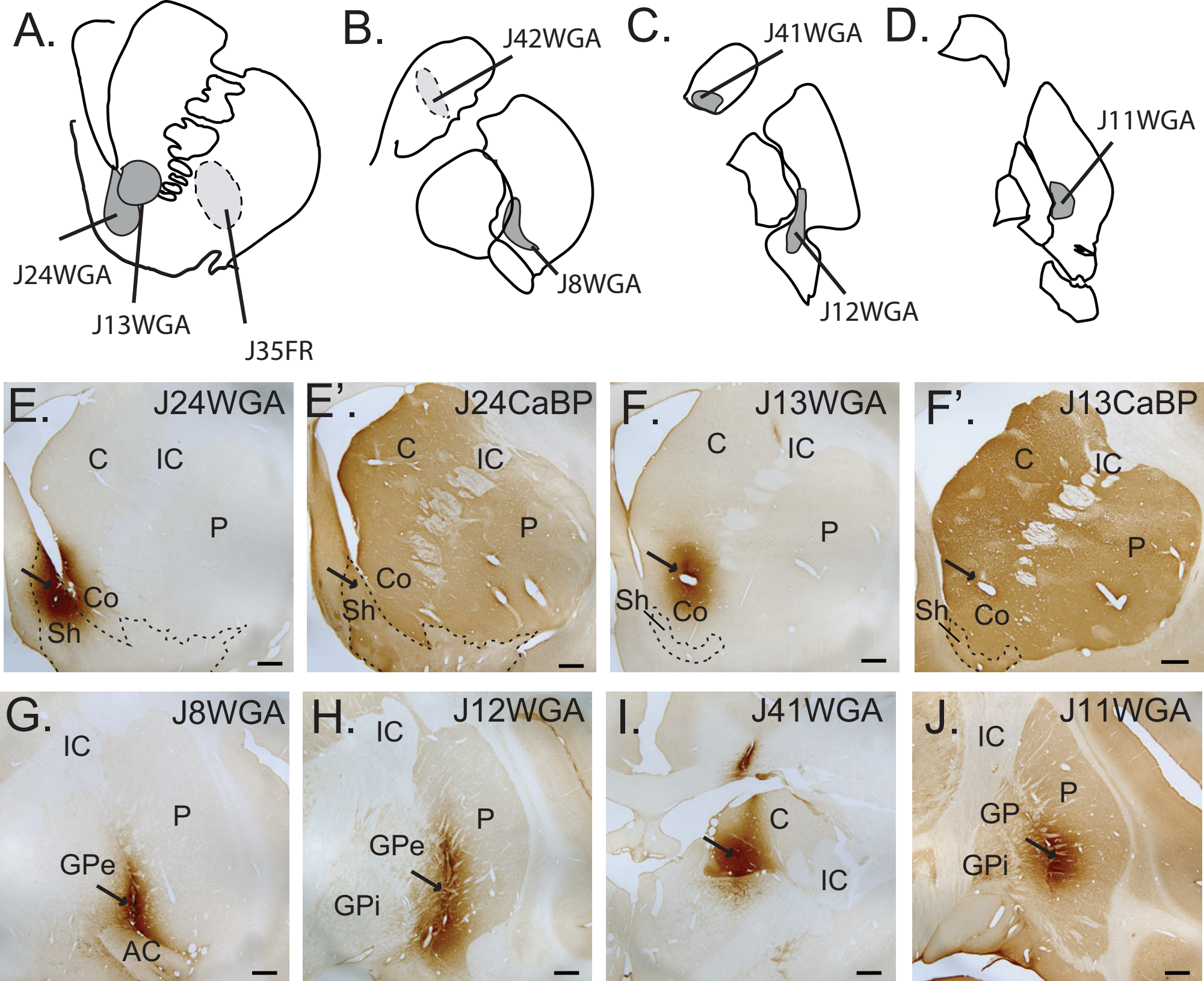
A.
J24WGA
J13WGA
J35FR
B.
J42WGA
J8WGA
C.
J41WGA
J12WGA
D.
J11WGA
E.
J24WGA
C
IC
P
Co
Sh
E'.
J24CaBP
C
IC
P
Co
Sh
F.
J13WGA
C
IC
P
Sh
Co
F'.
J13CaBP
C
IC
P
Sh
Co
G.
J8WGA
IC
P
GPe
AC
H.
J12WGA
IC
P
GPe
GPi
I.
J41WGA
C
IC
J.
J11WGA
IC
P
GP
GPi

A.

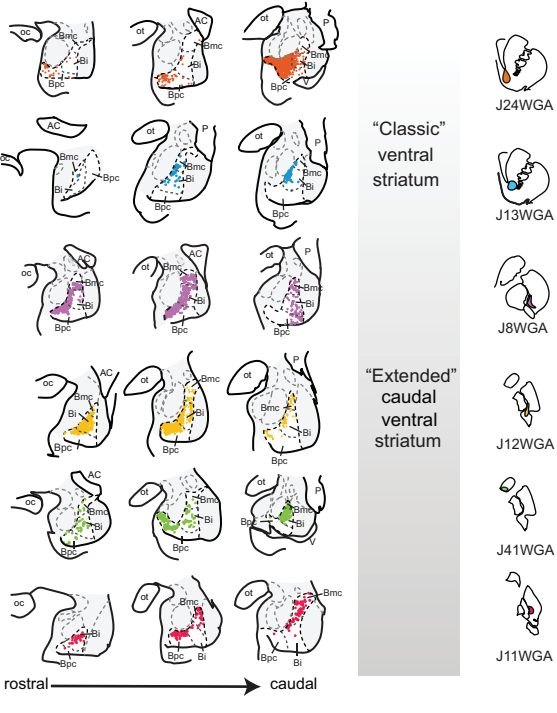
"Classic" ventral striatum
"Extended" caudal ventral striatum
J24WGA
J13WGA
J8WGA
J12WGA
J41WGA
J11WGA
rostral
caudal

B.

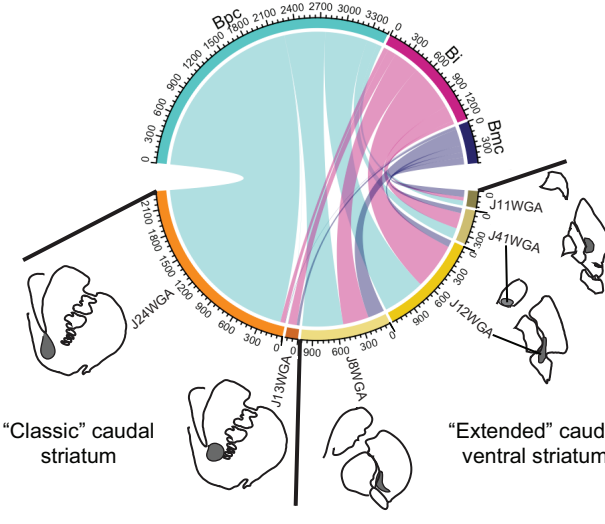
Bpc
Bi
Bmc
J11WGA
J41WGA
J12WGA
J8WGA
J13WGA
J24WGA
"Classic" caudal striatum
"Extended" caudal ventral striatum

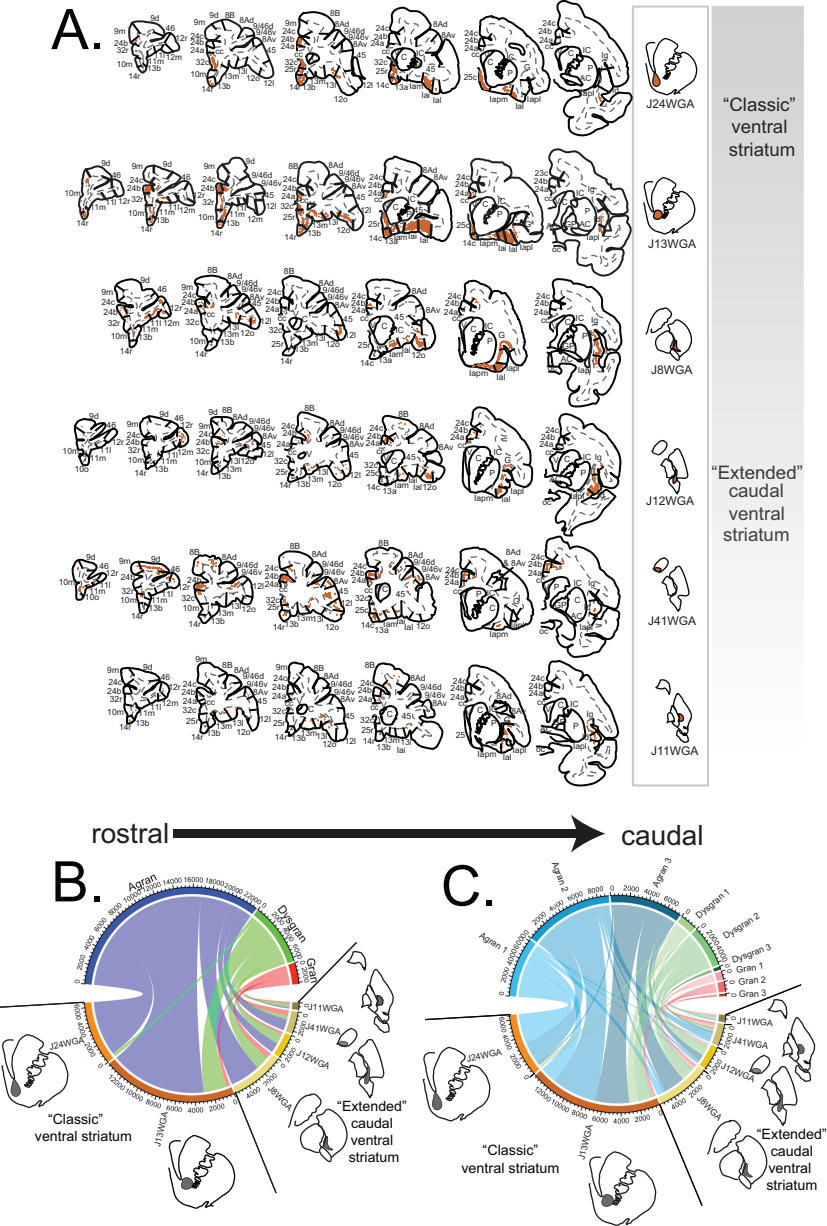
A.
J24WGA
J13WGA
J8WGA
J12WGA
J41WGA
J11WGA
"Classic" ventral striatum
"Extended" caudal ventral striatum
rostral
caudal
B.
Agran
Dysgran
Gran
J11WGA
J41WGA
J12WGA
J8WGA
J13WGA
J24WGA
"Classic" ventral striatum
"Extended" caudal ventral striatum
C.
Agran 2
Agran 3
Agran
Dysgran 1
Dysgran 2
Dysgran 3
Gran 1
Gran 2
Gran 3
J11WGA
J41WGA
J12WGA
J8WGA
J13WGA
J24WGA
"Classic" ventral striatum
"Extended" caudal ventral striatum

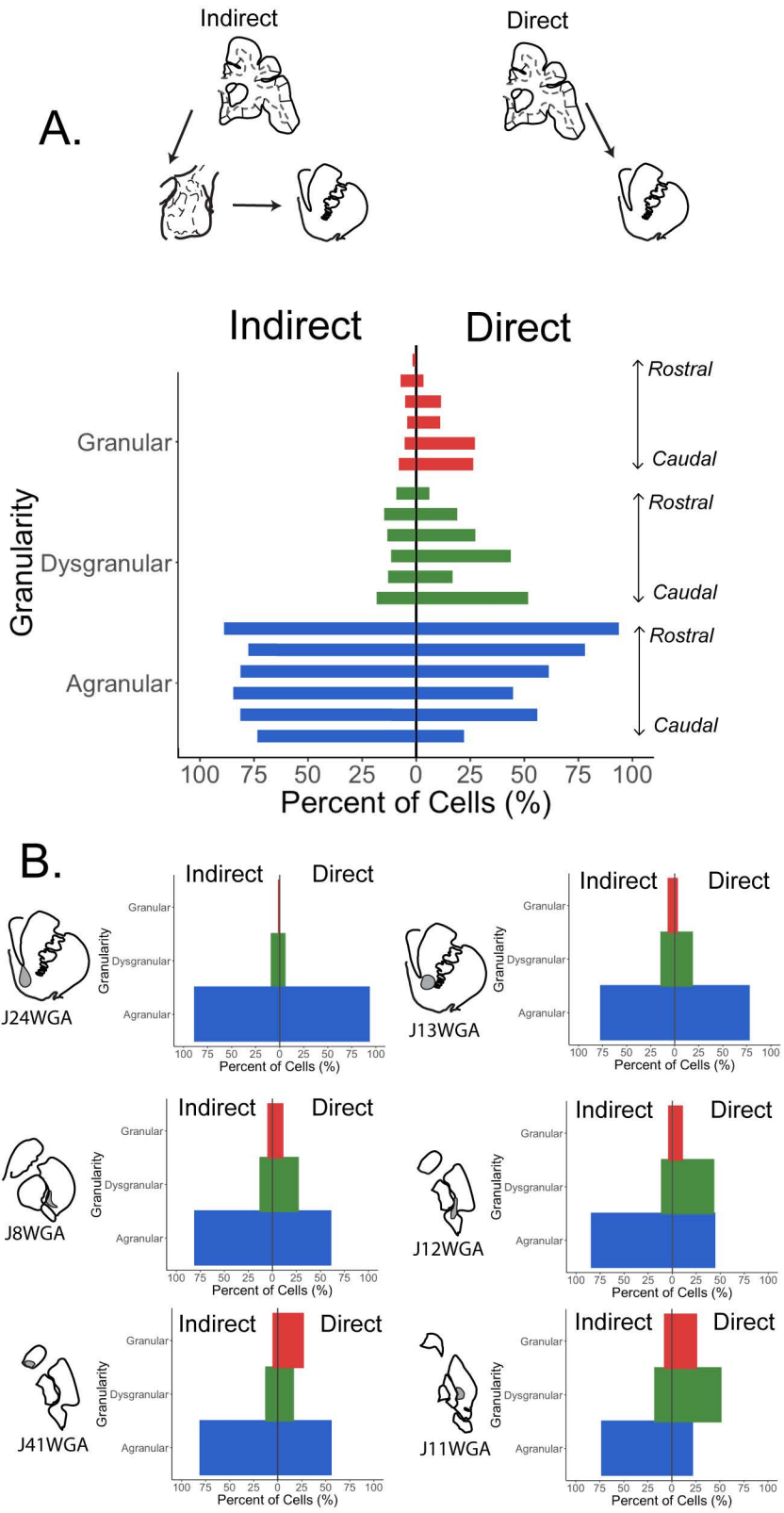
A.
Indirect
Direct
Indirect
Direct
Granularity
Granular
Dysgranular
Agranular
Rostral
Caudal
Rostral
Caudal
Rostral
Caudal
100 75 50 25 0 25 50 75 100
Percent of Cells (%)
B.
J24WGA
J13WGA
J8WGA
J12WGA
J41WGA
J11WGA
Indirect
Direct
Granularity
Granular
Dysgranular
Agranular
Percent of Cells (%)
C.
Percentage (%)
indirect
direct
Key
agranular indirect
dysgranular indirect
granular indirect
agranular direct
dysgranular direct
granular direct

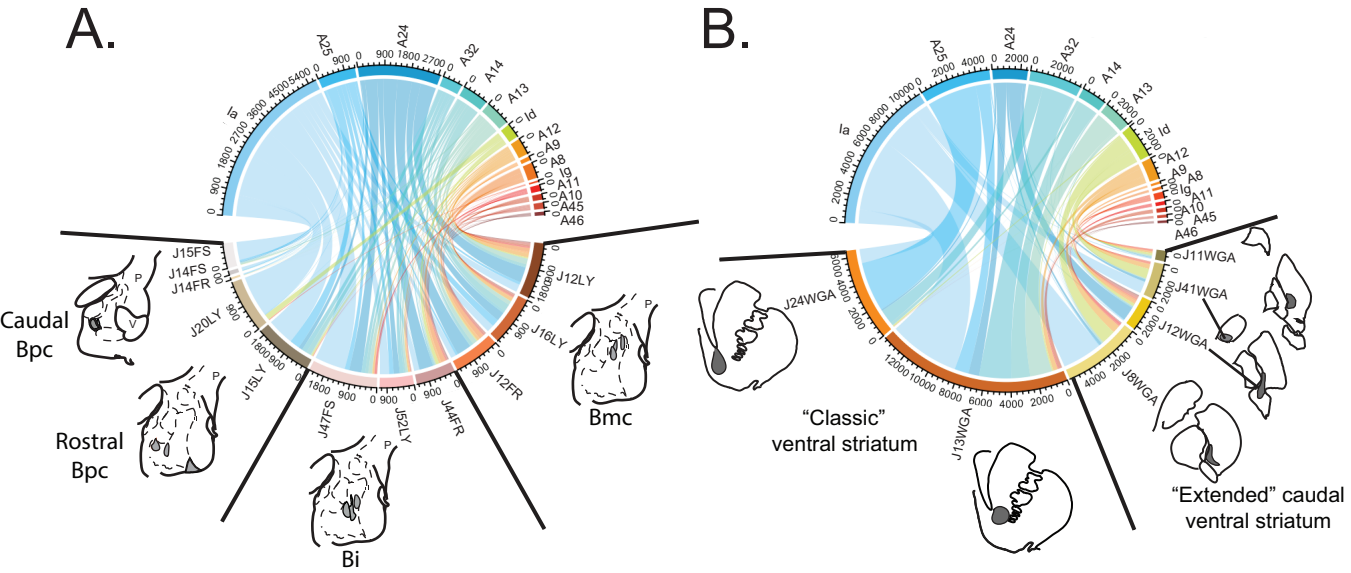
A.
B.
Caudal Bpc
Rostral Bpc
Bi
Bmc
"Classic" ventral striatum
"Extended" caudal ventral striatum
A25
A24
A32
A14
A13
Id
A12
A9
A8
Ig
A11
A10
A45
A46
J15FS
J14FS
J14FR
J20LY
J15LY
J47FS
J52LY
J44FR
J12FR
J16LY
J12LY
J24WGA
J13WGA
J8WGA
J12WGA
J41WGA
J11WGA
Ia

A.

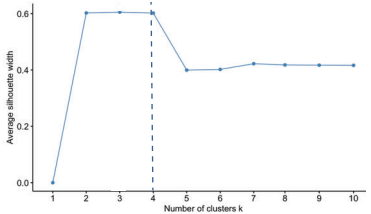

B.

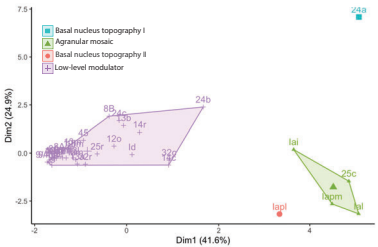

D.

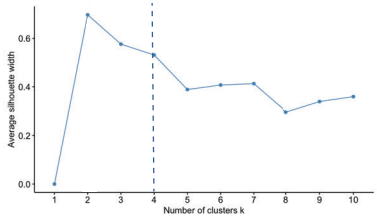

E.

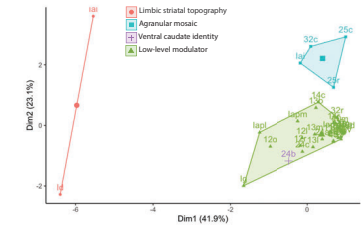

z-score color coding key:

-0.6000 - -0.1000
-0.0999 - -0.0001
0.0000 - 1.5000
1.5001 - 5.5000

C.

Basal nucleus topography I

		Bpc					Bi			Bmc			
Cortical area	Granularity	J15FS	J14FS	J14FR	J20LY	J15LY	J47FS	J52LY	J44FR	J12FR	J16LY	J12LY	AVERAGE
24a	Agran 1	-0.2534	-0.3870	-0.2587	-0.3022	0.4041	1.9075	0.9619	3.3613	5.1360	3.3088	4.8833	1.7056

Basal nucleus topography II

		Bpc					Bi			Bmc			
Cortical area	Granularity	J15FS	J14FS	J14FR	J20LY	J15LY	J47FS	J52LY	J44FR	J12FR	J16LY	J12LY	AVERAGE
Iapl	Agran 3	1.2126	2.6661	2.7326	5.2480	0.2454	-0.0810	0.0208	1.3811	-0.1858	-0.4915	-0.4557	1.1175

Agranular mosaic

		Bpc					Bi			Bmc			
Cortical area	Granularity	J15FS	J14FS	J14FR	J20LY	J15LY	J47FS	J52LY	J44FR	J12FR	J16LY	J12LY	AVERAGE
Iapm	Agran 1	3.0653	2.3503	1.2370	0.3426	2.1672	4.4038	-0.5567	-0.4172	-0.5026	1.1426	-0.2485	1.1803
25c	Agran 1	0.5199	2.1397	3.6300	-0.1821	2.6168	0.9003	2.5662	-0.5991	0.5428	2.1877	0.0702	1.3084
Iai	Agran 2	-0.0440	3.7189	-0.2587	0.4311	0.0691	2.4067	2.7587	-0.2758	0.5586	0.2496	1.6799	1.0267
Ial	Agran 3	4.6602	0.3500	1.2370	2.1252	4.2917	0.7540	2.0528	0.1283	0.3527	-0.1494	0.0065	1.4372

Low-level modulator

		Bpc					Bi			Bmc			
Cortical area	Granularity	J15FS	J14FS	J14FR	J20LY	J15LY	J47FS	J52LY	J44FR	J12FR	J16LY	J12LY	AVERAGE
Iam	Agran 1	-0.1245	-0.3870	-0.2587	-0.1505	-0.4158	-0.5200	-0.3642	-0.5789	-0.4550	0.0596	-0.5673	-0.3420
14c	Agran 1	-0.2534	0.5605	1.2370	-0.2390	0.6157	0.3064	0.2561	-0.4576	0.0676	0.8196	-0.5195	0.2176
32c	Agran 2	-0.2051	-0.3870	1.5361	-0.3022	-0.1425	0.3236	2.0528	0.2294	-0.3442	0.4396	-0.6470	0.2321
25r	Agran 2	-0.3017	-0.3870	0.3396	-0.3022	-0.3540	-0.5372	-0.4498	-0.6193	-0.5659	1.1236	-0.2007	-0.2050
24b	Agran 2	-0.2051	-0.3870	-0.5578	-0.3022	-0.0720	0.4958	2.3095	2.6136	0.7962	0.6486	0.9308	0.5700
13a	Agran 3	0.1171	-0.3870	-0.5578	-0.2959	-0.3893	-0.1670	0.2989	-0.6395	-0.5184	-0.7385	-0.5992	-0.3524
24c	Agran 3	-0.1245	-0.3870	-0.5578	-0.3022	-0.4422	-0.1584	-0.4925	2.1287	0.4794	-0.2825	0.6758	0.0488
32r	Dysgran 1	-0.3662	-0.3870	-0.5578	-0.3022	0.7743	-0.2273	-0.2573	-0.6193	-0.5184	-0.4345	-0.5195	-0.3105
12o	Dysgran 1	-0.3662	-0.3870	0.6387	-0.3022	-0.3012	-0.3995	-0.2359	-0.4778	0.1310	0.4586	0.3571	-0.0804
14r	Dysgran 1	-0.1890	-0.3870	-0.2587	-0.3022	-0.0102	-0.4253	-0.1075	-0.5991	0.2894	2.4917	0.4049	0.0825
13b	Dysgran 2	-0.1567	-0.3870	-0.5578	-0.3022	-0.4069	-0.3478	-0.1289	-0.2960	0.6061	0.9906	1.0902	0.0094
12r	Dysgran 2	-0.3662	-0.3870	-0.5578	-0.3022	-0.4598	-0.1584	-0.3642	-0.5991	-0.4392	-0.8145	-0.2963	-0.4313
13m	Dysgran 2	-0.2695	-0.3870	-0.5578	-0.3022	-0.3981	-0.4081	-0.5781	-0.5991	0.1627	-0.4725	-0.0254	-0.3486
Id	Dysgran 2	-0.2212	-0.1764	0.9378	0.9810	-0.0543	-0.4597	-0.4925	1.5831	-0.0749	-0.6625	-0.0414	0.1199
13l	Dysgran 3	-0.3178	-0.3870	-0.2587	-0.3022	-0.4246	-0.0379	-0.4925	-0.4778	-0.3600	-0.4915	-0.4238	-0.3613
8B	Dysgran 3	-0.3501	-0.3870	-0.5578	-0.3022	-0.4598	-0.5286	-0.5567	1.4619	1.4931	-0.6815	0.7077	-0.0146
9m	Dysgran 3	-0.3662	-0.3870	-0.5578	-0.3022	-0.4598	-0.4941	-0.3000	-0.5587	-0.5184	-0.7195	-0.1848	-0.4408
9d	Gran 1	-0.3662	-0.3870	-0.5578	-0.3022	-0.4686	-0.5114	-0.5995	-0.4374	-0.5026	-0.8525	-0.5195	-0.5004
Ig	Gran 1	-0.3662	-0.3870	-0.2587	-0.0999	-0.4686	-0.5372	-0.6637	-0.5385	-0.5976	-0.8145	-0.6948	-0.4933
11m	Gran 1	-0.3662	-0.3870	-0.5578	-0.3022	-0.3893	-0.4167	-0.5995	-0.4576	-0.4550	-0.7195	-0.4557	-0.4642
11l	Gran 1	-0.3662	-0.3870	-0.5578	-0.3022	-0.4246	-0.0379	-0.4925	-0.4172	-0.5342	-0.4535	-0.5195	-0.4084
10o	Gran 2	-0.3662	-0.3870	-0.5578	-0.3022	-0.4686	-0.5114	-0.6423	-0.6395	-0.3917	-0.7575	-0.3601	-0.4895
10m	Gran 2	-0.3501	-0.3870	-0.2587	-0.3022	-0.4422	-0.5286	-0.5781	-0.2960	-0.2967	-0.0164	-0.1848	-0.3310
12m	Gran 2	-0.3662	-0.3870	-0.5578	-0.3022	-0.4686	-0.5286	-0.6637	-0.4374	-0.5501	-0.3775	-0.5832	-0.4748
12l	Gran 2	-0.3662	-0.3870	-0.5578	-0.3022	-0.4686	-0.4941	-0.3214	0.0879	-0.2967	-0.4155	-0.4398	-0.3601
45	Gran 2	-0.3662	-0.3870	-0.5578	-0.3022	-0.4686	-0.3650	-0.5139	-0.2758	0.1468	-0.2444	0.4686	-0.2605
8Av	Gran 3	-0.3662	-0.3870	-0.5578	-0.3022	-0.4686	-0.5114	-0.6423	-0.3768	-0.3125	-0.5865	-0.5195	-0.4573
8Ad	Gran 3	-0.3501	-0.3870	-0.5578	-0.3022	-0.4686	-0.5200	-0.4711	0.0273	-0.5659	-0.5675	-0.3601	-0.4112
46	Gran 3	-0.3662	-0.3870	-0.5578	-0.3022	-0.4686	-0.5372	-0.5353	-0.1748	-0.5501	-0.7575	-0.5673	-0.4731
9/46d	Gran 3	-0.3662	-0.3870	-0.5578	-0.3022	-0.4598	-0.5372	-0.6209	-0.5789	-0.5817	-0.7765	-0.6470	-0.5287
9/46v	Gran 3	-0.3662	-0.3870	-0.5578	-0.3022	-0.4598	-0.5114	-0.5567	-0.5587	-0.6451	-0.6435	-0.6948	-0.5166

F.

Limbic striatal topography

		'Classic'		'Extended'			
Cortical area	Granularity	J24WGA	J13WGA	J8WGA	J12WGA	J41WGA	J11WGA	AVERAGE
Ial	Agran 3	-0.1459	4.3088	4.7862	2.6223	-0.4616	-0.0349	1.8458
Id	Dysgran 2	-0.1277	-0.3756	2.7259	4.6639	1.0562	4.2188	2.0269

Agranular mosaic

		'Classic'		'Extended'			
Cortical area	Granularity	J24WGA	J13WGA	J8WGA	J12WGA	J41WGA	J11WGA	AVERAGE
25c	Agran 1	5.3613	-0.2015	-0.2925	-0.4435	-0.2061	-0.5043	0.6189
32c	Agran 2	1.4908	2.4415	-0.4105	-0.4158	-0.2813	-0.4749	0.3916
25r	Agran 2	0.9355	0.6839	-0.4220	-0.4573	-0.4390	-0.5923	-0.0485
Iai	Agran 2	1.2250	1.7888	0.1794	-0.3743	-0.0709	-0.3576	0.3984

Ventral caudate identity

		'Classic'		'Extended'			
Cortical area	Granularity	J24WGA	J13WGA	J8WGA	J12WGA	J41WGA	J11WGA	AVERAGE
24b	Agran 2	-0.1677	0.2976	-0.0594	-0.0421	5.4591	-0.3869	0.8501

Low-level modulator

		'Classic'		'Extended'			
Cortical area	Granularity	J24WGA	J13WGA	J8WGA	J12WGA	J41WGA	J11WGA	AVERAGE
Iam	Agran 1	-0.3207	-0.4327	-0.1256	-0.3743	-0.3940	-0.3282	-0.3292
Iapm	Agran 1	-0.2533	-0.1312	0.7607	-0.0836	-0.3940	-0.2109	-0.0521
24a	Agran 1	-0.2333	-0.3083	-0.3788	-0.2082	0.3123	-0.0349	-0.1419
14c	Agran 1	-0.1495	1.0600	-0.3241	-0.4089	-0.1084	-0.3576	-0.0481
Iapl	Agran 3	-0.1550	-0.2556	1.0887	0.7399	-0.3864	0.5518	0.2639
13a	Agran 3	-0.3207	-0.2132	-0.4076	-0.4504	-0.3864	-0.4163	-0.3658
24c	Agran 3	-0.3134	-0.4064	-0.2608	0.1932	0.8984	0.2878	0.0665
32r	Dysgran 1	-0.1204	0.1000	-0.4076	-0.4712	-0.2061	-0.5923	-0.2829
12o	Dysgran 1	-0.2897	-0.1693	0.0125	0.8991	-0.3038	0.9919	0.1901
14r	Dysgran 1	-0.0585	-0.0654	-0.4277	-0.4712	-0.4240	-0.2109	-0.2763
13b	Dysgran 2	-0.3207	1.0424	-0.4248	-0.4435	-0.4541	0.0238	-0.0961
12r	Dysgran 2	-0.3207	-0.5322	0.0068	0.1171	-0.3414	0.5518	-0.0864
13m	Dysgran 2	-0.3207	-0.0917	-0.3443	-0.1459	-0.4315	0.2878	-0.1744
13l	Dysgran 3	-0.2952	-0.4547	-0.2436	-0.4089	-0.3188	0.8159	-0.1509
8B	Dysgran 3	-0.3207	-0.5454	-0.4191	-0.3674	0.0268	-0.1816	-0.3012
9m	Dysgran 3	-0.3207	-0.5410	-0.4277	-0.4296	-0.3338	-0.5043	-0.4262
9d	Gran 1	-0.3207	-0.5439	-0.4277	-0.4504	0.5002	-0.5923	-0.3058
Ig	Gran 1	-0.3152	-0.5410	-0.1457	0.6085	0.1620	3.2214	0.4983
11m	Gran 1	-0.3207	-0.4517	-0.3385	-0.4504	-0.4390	-0.5336	-0.4223
11l	Gran 1	-0.3207	-0.5425	-0.0652	-0.4435	-0.3714	-0.2109	-0.3257
10o	Gran 2	-0.3207	-0.5410	-0.4277	-0.4435	-0.4616	-0.5923	-0.4645
10m	Gran 2	-0.2970	-0.1942	-0.4162	-0.4504	-0.2437	-0.5923	-0.3656
12m	Gran 2	-0.3207	-0.5249	-0.3644	-0.3604	-0.4616	-0.3576	-0.3983
12l	Gran 2	-0.3207	-0.4268	0.3521	-0.0905	-0.0784	0.1705	-0.0657
45	Gran 2	-0.3207	-0.5454	-0.3673	-0.2774	0.7030	-0.5336	-0.2236
8Av	Gran 3	-0.3207	-0.5454	-0.4162	-0.4573	-0.1310	-0.2989	-0.3616
8Ad	Gran 3	-0.3188	-0.5454	-0.4162	-0.4573	-0.2888	-0.5923	-0.4365
46	Gran 3	-0.3207	-0.5059	-0.3184	-0.4573	-0.3038	-0.5923	-0.4164
9/46d	Gran 3	-0.3207	-0.5454	-0.4248	-0.4573	-0.4465	-0.5336	-0.4547
9/46v	Gran 3	-0.3207	-0.5454	-0.4076	-0.4504	0.0493	-0.5043	-0.3632

Total cell count per injection site data for Z-scoring

Injection site ID	Retrograde path	Mean	Standard Deviation
J15FS	Cortico-amygdala	22.73	62.07
J14FS	Cortico-amygdala	3.68	9.50
J14FR	Cortico-amygdala	1.86	3.34
J20LY	Cortico-amygdala	47.81	158.19
J15LY	Cortico-amygdala	53.16	113.44
J47FS	Cortico-amygdala	62.41	116.17
J52LY	Cortico-amygdala	31.03	46.75
J44FR	Cortico-amygdala	35.65	49.49
J12FR	Cortico-amygdala	41.73	63.14
J16LY	Cortico-amygdala	44.86	52.63
J12LY	Cortico-amygdala	50.59	62.75
J24WGA	Cortico-striatal	176.14	549.28
J13WGA	Cortico-striatal	372.68	683.32
J8WGA	Cortico-striatal	148.65	347.53
J12WGA	Cortico-striatal	68.08	144.50
J41WGA	Cortico-striatal	61.43	133.09
J11WGA	Cortico-striatal	20.19	34.09

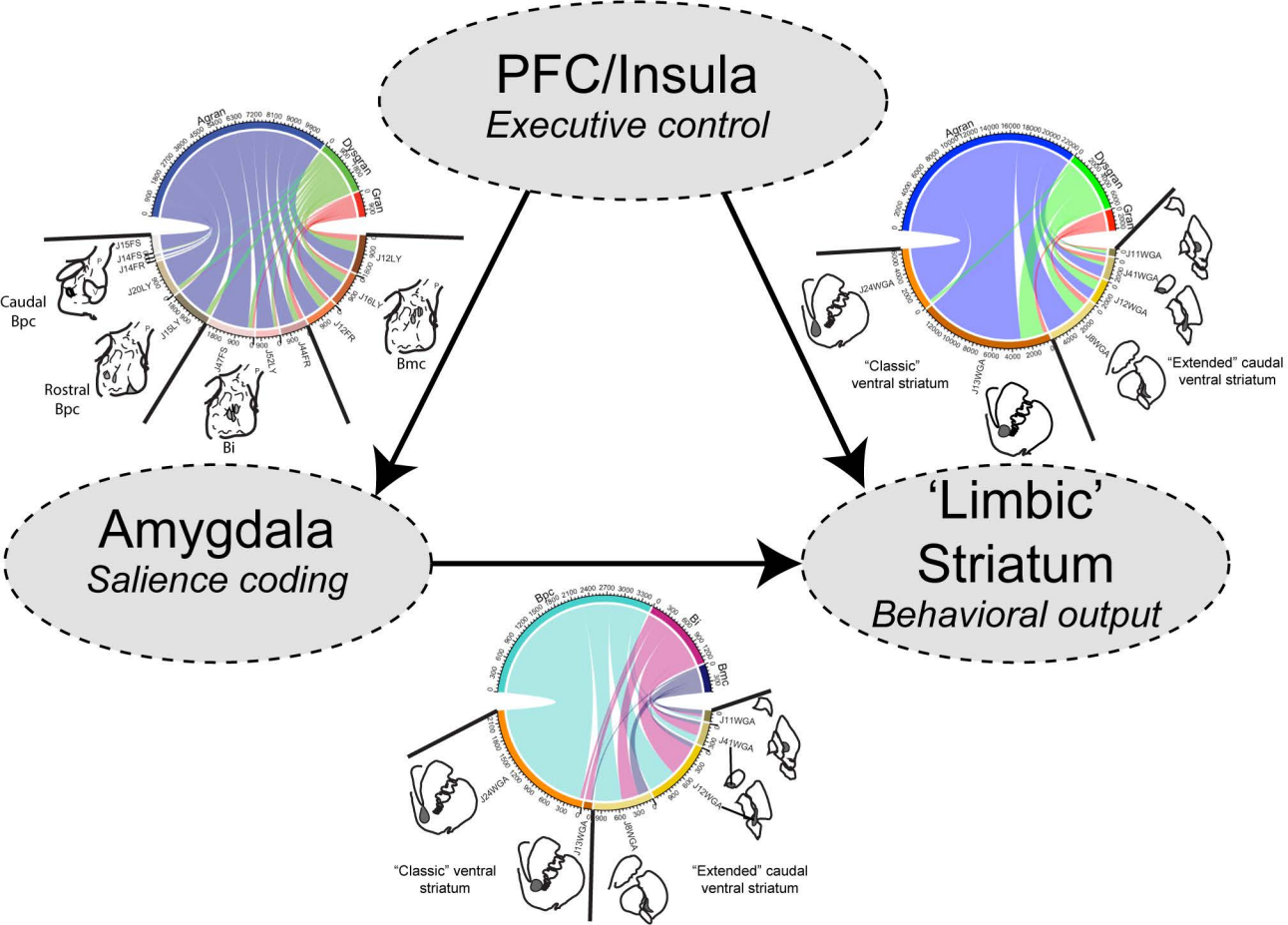
PFC/Insula
Executive control
Amygdala
Salience coding
'Limbic' Striatum
Behavioral output
Agran
Dysgran
Gran
Caudal Bpc
Rostral Bpc
Bi
Bmc
"Classic" ventral striatum
"Extended" caudal ventral striatum
Bpc
Bi
Bmc
J11WGA
J41WGA
J12WGA
J8WGA
J13WGA
J24WGA
J15FS
J14FS
J14FR
J20LY
J15LY
J16LY
J12LY
J12FR
J4FR
J52LY
J47FS